BEHAVIOR OF CANTILEVER BEAM UNDER IMPACT BY A SOFT PROJECTILE

Stephen W. Tsai, et al

Air Force Materials Laboratory
Wright-Patterson Air Force Base, Ohio

November 1974

NOTICE

When Government drawings, specifications, or other data are used for any purpose other than in connection with a definitely related Government procurement operation, the United States Government thereby incurs no responsibility nor any obligation whatsoever; and the fact that the government may have formulated, furnished, or in any way supplied the said drawings, specifications, or other data, is not to be regarded by implication or otherwise as in any manner licensing the holder or any other person or corporation, or conveying any rights or permission to manufacture, use, or sell any patented invention that may in any way be related thereto.

This report has been reviewed and cleared for open publication and/or public release by the appropriate Office of Information (OI) in accordance with AFR 190-17 and DODD 5230.9. There is no objection to unlimited distribution of this report to the public at large, or by DDC to the National Technical Information Service (NTIS).

This technical report has been reviewed and is approved for publication.

STEPHEN W TSAI

FOR THE COMMANDER

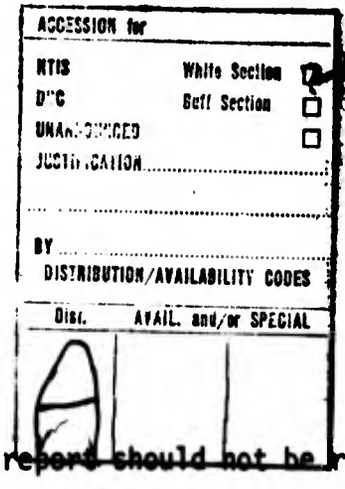

STEPHEN W TSAI
Chief, Mech & Surface Interactions Br

Copies of this report should not be returned unless return is required by security considerations, contractual obligations, or notice on a specific document.

UNCLASSIFIED

SECURITY CLASSIFICATION OF THIS PAGE *(When Data Entered)*

REPORT DOCUMENTATION PAGE		READ INSTRUCTIONS BEFORE COMPLETING FORM
1. REPORT NUMBER AFML-TR-74-94	2. GOVT ACCESSION NO.	3. RECIPIENT'S CATALOG NUMBER AD-A008 778
4. TITLE *(and Subtitle)* BEHAVIOR OF CANTILEVER BEAM UNDER IMPACT BY A SOFT PROJECTILE		5. TYPE OF REPORT & PERIOD COVERED 6. PERFORMING ORG. REPORT NUMBER
7. AUTHOR(s) S. W. Tsai H. T. Hahn C. T. Sun T. W. Lee A. K. Hopkins		8. CONTRACT OR GRANT NUMBER(s)
9. PERFORMING ORGANIZATION NAME AND ADDRESS Air Force Materials Laboratory Air Force Systems Command Wright-Patterson Air Force Base, Ohio 45433		10. PROGRAM ELEMENT, PROJECT, TASK AREA & WORK UNIT NUMBERS 7340/73400207
11. CONTROLLING OFFICE NAME AND ADDRESS		12. REPORT DATE November 1974 13. NUMBER OF PAGES
14. MONITORING AGENCY NAME & ADDRESS(if different from Controlling Office)		15. SECURITY CLASS. (of this report) Unclassified 15a. DECLASSIFICATION DOWNGRADING SCHEDULE

16. DISTRIBUTION STATEMENT *(of this Report)*

Approved for public release; distribution unlimited.

17. DISTRIBUTION STATEMENT *(of the abstract entered in Block 20, if different from Report)*

18. SUPPLEMENTARY NOTES

19. KEY WORDS *(Continue on reverse side if necessary and identify by block number)*

Composite, Laminate, Impact Behavior, Cantilever Beam, Coefficient of Restitution, Foreign Object Damage, Impulsive Loading

20. ABSTRACT *(Continue on reverse side if necessary and identify by block number)*

In an attempt to determine the maximum deflection and the ultimate strength of a fan blade under the impact of a bird, experiments were performed on the impact of cantilever beams by soft-rubber projectiles. The observed response of the projectile and beam can be correlated with a simple analytic model - an equivalent mass-spring system which is derived from an assumed deflection mode. The initial velocity of the equivalent mass immediately after impact is computed from the momentum conservation principle and measured coefficient of

DD FORM 1 JAN 73 1473 EDITION OF 1 NOV 65 IS OBSOLETE

UNCLASSIFIED

SECURITY CLASSIFICATION OF THIS PAGE *(When Data Entered)*

restitution. This information and the dynamic characteristics of the equivalent mass-spring system are shown to be fairly sufficient to predict the behavior of the beam. The success of this model implies that the structural response of fan blades under bird impact can be made predictable.

FOREWORD

This final report was prepared by the Air Force Materials Laboratory, Wright-Patterson Air Force Base, Ohio 45433. Stephen W. Tsai was the laboratory project monitor.

Research was conducted under Project 7351, "Metallic Materials for Air Force Weapon Systems Components," Task 735106, "Behavior of Metals Used in Flight Vehicle and Engine Structural Applications," and Project 7340, "Nonmetallic and Composite Materials," Task 734003, "Structural Plastics and Composites."

This report covers work performed during the period of January 1973 through August 1973. This manuscript was released by the authors in January 1974.

This work was participated in by Drs. C. T. Sun and H. T. Hahn, National Research Council Post Doctoral Associates assigned to the Air Force Materials Laboratory. Their participation in this investigation was part of their research activities. Dr. Sun was on sabbatical leave from the Department of Mechanics and Engineering Sciences of the Iowa State University, Ames, Iowa, when he served his NRC tenure at the Air Force Materials Laboratory.

TABLE OF CONTENTS

LIST OF ILLUSTRATIONS

LIST OF FIGURES CONTINUED

LIST OF TABLES

LIST OF SYMBOLS

A	amplitude of y
A_i	$= [y]_{t=0}$
A_m	$= [A]_{v=v_m}$
B	amplitude of ϕ
b	width of beam
c	distance between centroid and center of mass
E	Young's modulus of beam
e	coefficient of restitution
G	shear modulus of beam
$H(H')$	height of sphere before (after) impact
h	thickness of beam
$I(I_o)$	minimum area moment of inertia (at root)
I_T	$= bh^3/3$
J	polar mass moment of inertia
$K(K_T)$	effective flexural (torsional) stiffness
L	length of beam
$M(M_T)$	effective mass for bending (torsion)
M_b	total mass of beam
m	mass of foreign object
P	concentrated force
T	torque
t	time
V	velocity of effective mass after impact
$v(v')$	velocity of foreign object before (after) impact

LIST OF SYMBOLS (CONTINUED)

v_n	normal component of v
v_m	v which causes failure of beam
X	coordinate along the axis of beam
x	location of impact
Y	flexural deflection
y	$= [Y]_{X=x}$
z	distance between point of impact and center of mass
α	shape factor
γ	phase angle
δ	Y at tip
δ_m	$= [\delta]_{v=v_m}$
θ	incident angle
$\rho(\rho_c)$	mass per unit length (at root)
α	stress
Φ	angle of twist
ϕ	$= [\Phi]_{X=x}$
Ω	initial angular velocity
$\omega(\omega_T)$	flexural (torsional) natural frequency

SECTION I

INTRODUCTION

Foreign object damage (FOD) has been recognized as the number one barrier against the use of advanced composites in fan blades. While numerous development programs in the past decade have demonstrated the advantages of composites, the following examples are deemed worthwhile repeating:

1. Weight of fan blades is a major controlling factor which determines size or weight of remaining structures such as wheels, shafts, bearings, and containment support structures. One pound savings in blades may multiply to six pounds in total system. Weight savings has direct impact on payload, range and cost.

2. Higher specific modulus and higher specific strength of composites will increase fan efficiency through the use of higher tip speed, wider chord (lower aspect ratio), elimination of mid-span shrouds, and wider range of flutter-free design. All the features of composite blades are essentially additive, resulting in significant improvement in the overall fan operation.

In experimental engines, Pratt & Whitney Aircraft has produced first-stage blades with up to 63 percent savings in weight by using graphite-polyimide over titanium blades. General Electric also demonstrated over 30 percent weight savings in their TF 39 fan rotor using graphite-epoxy composites (Reference 1). The Rolls-Royce RB 211 engine would have 25 Hyfil blades weighting 9.2 pounds each as compared with 33 titanium blades at 16.5 pounds each (Reference 2). The wider chord of Hyfil blades permits the use of fewer blades. The total difference in weight of blades is 230 pounds for Hyfil over 545 pounds for titanium or a 58% savings.

It is the purpose of this investigation to develop an effective laboratory technique to determine the structural behavior and strength of blades during impact by a soft object. Cantilever beams made of

representative composites were impacted by soft rubber projectiles. The experimental observations were checked against an analytical model based on an equivalent mass-spring system. It can be concluded that the structural behavior and strength of blades, stationary or rotating, can be predicted when impacted by small soft objects such as birds.

In Section II, an analytical model of a mass-spring system will be developed in detail. In Section III, the experimental facility, instrumentation, and resulting data will be reported. Discussion based on the comparision between data and theory will be covered in Section IV. Conclusions and recommendations for future work will be cited in Section V. Several appendices are included to show detailed description of the coefficient of restitution, the case of torsional deflection and frequency, and sample calculations.

SECTION II

ANALYTICAL MODEL

For analysis purposes the blade is frequently considered to be a cantilever beam with lumped masses placed at selected locations (Figure 1). The number of degrees of freedom of the lumped mass-spring system depends on the geometrical properties of the blade as well as the accuracy of analysis required. As a preliminary step, however, we here replace the blade by only one lumped mass M, with the polar mass moment of inertia, J, located at the point of impact (Figure 2). The stiffness of the blade is represented by a linear spring k and a torsional spring k_T. In Figure 2, m, v and x represent, respectively, the mass, impact velocity of the foreign object, and the location of impact. The quantities M, J, k, k_T are in general functions of the following variables: the location of impact, the distribution of area and polar moments of inertia, the density per unit length $\rho(X)$, the Young's modulus $E(X)$ and shear modulus $G(X)$, and the deflections assumed.

In Figure 2, C and C_G respectively denote the centroid and center of mass, while y and ϕ represent the linear displacement and the angular rotation, respectively. The kinetic and the potential energies of the system are given by

$$T = \frac{1}{2} M (\dot{y} - c\dot{\phi})^2 + \frac{1}{2} J\dot{\phi}^2$$

$$V = \frac{1}{2} ky^2 + \frac{1}{2} k_T\phi^2 \qquad (1)$$

Using Lagrange's method, we obtain the equations of motion of the system

$$\begin{bmatrix} M & -cM \\ -cM & J+c^2M \end{bmatrix} \begin{Bmatrix} \ddot{y} \\ \ddot{\phi} \end{Bmatrix} + \begin{bmatrix} k & 0 \\ 0 & k_T \end{bmatrix} \begin{Bmatrix} y \\ \phi \end{Bmatrix} = \begin{Bmatrix} 0 \\ 0 \end{Bmatrix} \qquad (2)$$

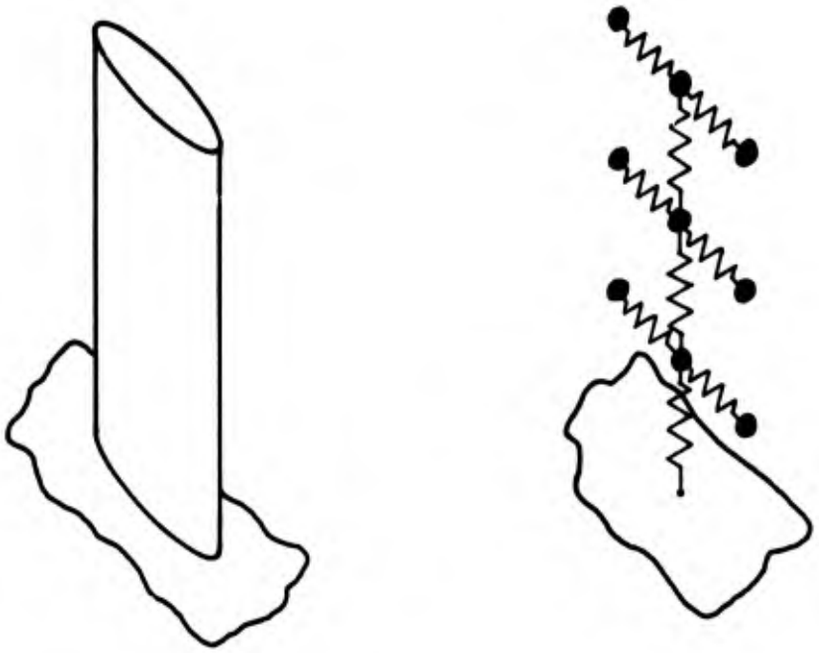

Figure 1. Simulation of Actual Blade by Lump Parameter Model

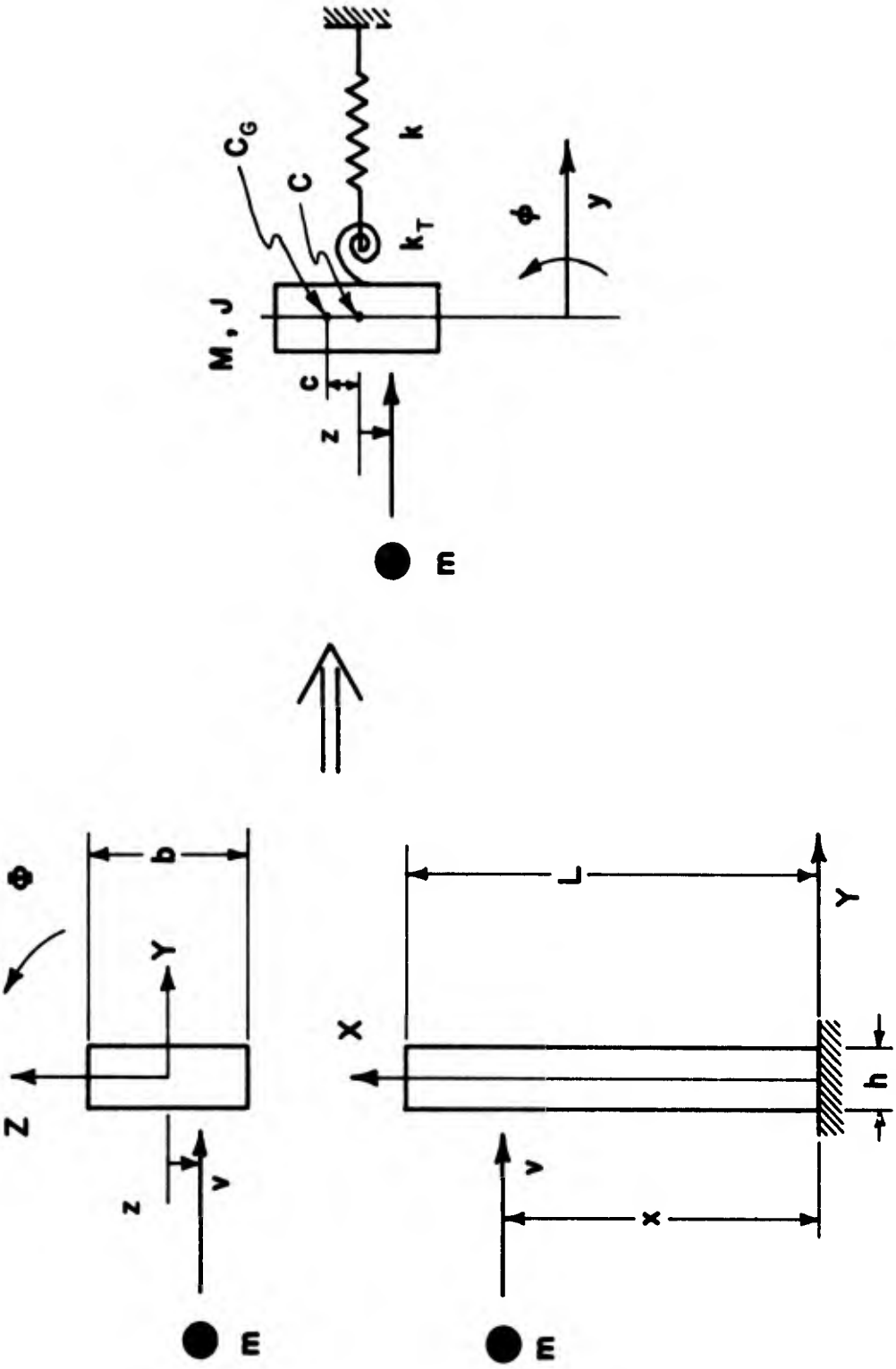

Figure 2. A Two-Lump Parameter Model for Cantilever Beam

It is evident from Equation 2 that the motion of the system is coupled through c. The terms with c appear only in the off-diagonal terms of the mass matrix: physically this implies that the coupling is dynamic, i.e., if the system is displaced by a force at C and released, the inertia force which acts at C_G will result in a moment about C and produce a rotation superimposed on the translation. Thus, if the center of mass coincides with the centroid, then the modes of flexural and torsional vibration are uncoupled, and each mode will behave independently. Otherwise, dynamic coupling will result.

For most blade geometries considered, the distance between the centroid and the center of mass is very small, rendering possible independent consideration of each mode of vibration. Therefore, in this report, coupling is neglected, leading to the mass-spring model shown in Figure 3. Moreover, only the flexural vibration will be discussed in detail. The uncoupled torsional vibration is briefly described in Appendix II.

1. EFFECTIVE FLEXURAL STIFFNESS k

In this section we derive the effective stiffness k as a function of the minimum area moment of inertial I_0, the Young's modulus E of the blade, and the location of impact $\frac{X}{L}$. In general, there are two methods available.

One method is to equate the maximum potential energy of the blade system with the maximum potential energy of the mass-spring system, i.e.,

$$\frac{1}{2} \int_0^L E(X)\, I(X)\, \frac{d^2 Y}{dX^2}\, dX = \frac{1}{2}\, k\, y^2 \qquad (3)$$

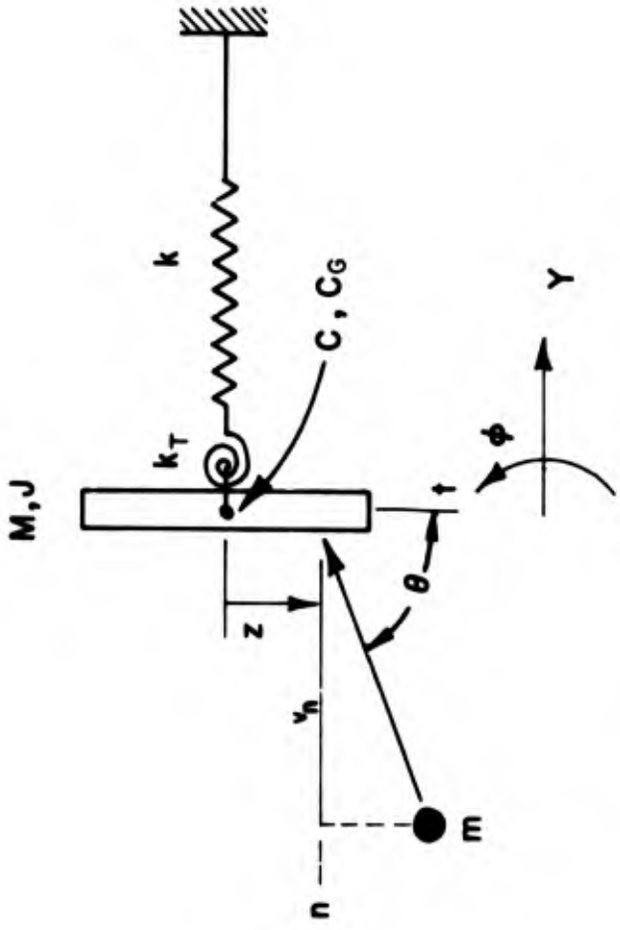

Figure 3. Uncoupled Two-Lump Model Impacted by a Projectile with Oblique Incidence

where Y = Y (X) is assumed to be the static deflection curve under a concentrated load at the point of impact. Another method is to use the definition of k., i.e.,

$$k = \left[\frac{P}{Y(X)}\right]_{X=x} \tag{4}$$

where P is the applied concentrated force at x.

The static deflection curve can be determined from the well known formula

$$\frac{d^2Y}{dX^2} = \frac{P(x-X)}{E(X)\ I(X)}, \quad 0 \leq X \leq x$$

$$\frac{d^2Y}{dX^2} = 0 \qquad\qquad x \leq X \leq L \tag{5}$$

Two different cases which appear to represent the actual blades are considered:

(1) E = Constant, $I = I_0$ = Constant

(2) E = Constant, $I = I_0 (1 - \frac{X}{L})^2$

The first case corresponds to a homogeneous beam with uniform cross section and the second case to an idealized distribution of I(X) for stainless steel, boron-aluminum, graphite-epoxy, and titanium blades. The distribution I(X) are shown for these blades in Figure 4-a. We now derive Y as a function of X for each case separately.

Case (1) E = Constant $I = I_0$ = Constant

For this case, Y can be determined in a straightforward manner by double integration with respect to X and by using the boundary conditions at X = 0, and the continuity at X = x., i.e.,

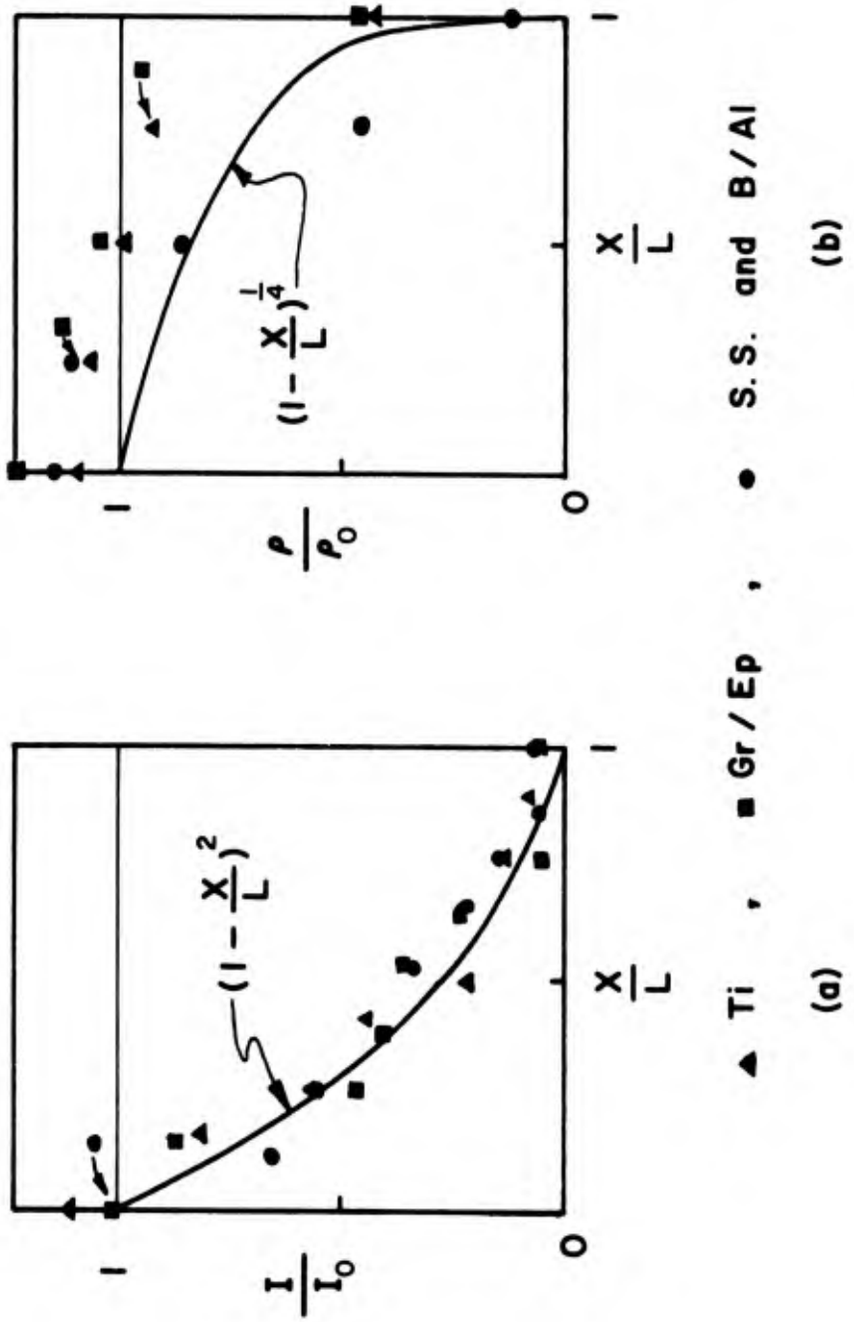

Figure 4. Distribution per Unit Length of: (a) Area Moment of Inertia; (b) Mass Density

$$Y = 0 \quad \text{at } X = 0$$

$$\frac{dY}{dX} = 0 \quad \text{at } X = 0$$

$$Y \text{ is continuous at } X = x \tag{6}$$

$$\frac{dY}{dX} \text{ is continuous at } X = x$$

The final expression for Y is given by

$$Y = \frac{1}{2} y \left[3 \left(\frac{X}{x}\right)^2 - \left(\frac{X}{x}\right)^3\right] \quad 0 \le X \le x$$

$$Y = y \left[1 + \frac{3}{2} \left(\frac{X}{x} - 1\right)\right] \quad x \le X \le L \tag{7}$$

where y is the deflection at X = x:

$$y = \frac{PL^3}{3EI_0} \left(\frac{x}{L}\right)^3 \tag{8}$$

From Equations 4 and 8 follows

$$k = \frac{3EI_0}{x^3} = \frac{3EI_0}{L^3} \left(\frac{L}{x}\right)^3 \tag{9}$$

The stiffness k is plotted as a function of $\frac{X}{L}$ in Figure 5.

Case (2) E = Constant, $I = I_0 (1 - \frac{X}{L})^2$

Substituting the expression for I(X) into Equation 5 and solving the resulting differential equation, we obtain

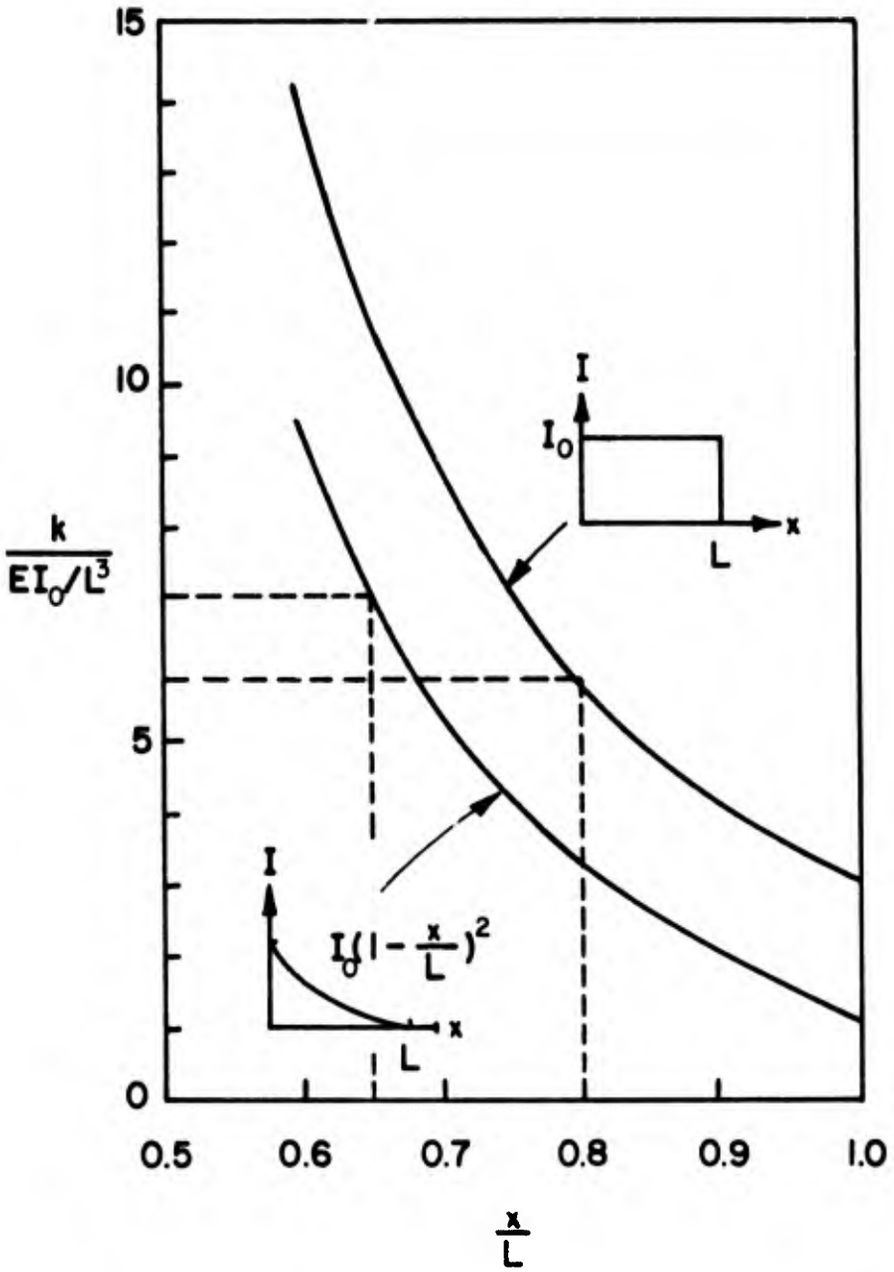

Figure 5. Effective Flexural Stiffness versus Location of Impact

$$Y = \alpha y \left(\frac{L}{x}\right)^2 \left[2\frac{X}{x} - \frac{X}{L} + \left(2\frac{L}{x} - \frac{X}{x} - 1\right) \ell n\left(1 - \frac{X}{L}\right)\right] \qquad (10)$$

$$0 \leq X \leq x$$

where

$$y = \frac{PL^3}{\alpha EI_0}\left(\frac{x}{L}\right)^3 \qquad (11)$$

$$\alpha = \left(\frac{x}{L}\right)^2 \left[2 - \frac{x}{L} + 2\left(\frac{L}{x} - 1\right) \ell n \left(1 - \frac{x}{L}\right)\right]^{-1}. \qquad (12)$$

The stiffness k can then be evaluated from Equations 4 and 11 as

$$k = \frac{P}{y} = \frac{\alpha EI_0}{L^3}\left(\frac{L}{x}\right)^3 \qquad (13)$$

Comparison of Equation 13 with Equation 9 reveals that α is a "shape factor" showing the effect of the distribution of moment of inertia. Figure 5 shows k as a function of x/L. In both cases k is seen to increase with L/x. This implies that as the location of impact is closer to the root of the blade, the effective stiffness increases.

The equation for Y in the interval $x \leq X \leq L$ can be obtained from Equations 5, 10, and the conditions of continuity as given by Equation 6:

$$Y = y\left\{1 - \alpha\left(\frac{L}{x}\right)^2 \left[1 + \frac{L}{x} \ell n\left(1 - \frac{x}{L}\right)\right]\left(\frac{X}{L} - \frac{x}{L}\right)\right\} \qquad (14)$$

$$x \leq X \leq L$$

2. EFFECTIVE FLEXURAL MASS M

To determine the effective mass M as a function of the location of impact, we equate the maximum kinetic energy of the actual blade to the maximum kinetic energy of the mass-spring system. The maximum kinetic

energy of the blade is given by

$$T_1 = \frac{1}{2} \int_0^L \dot{Y}(X)^2 \rho(X)\, dX \tag{15}$$

and the maximum kinetic energy of the mass-spring system is given by

$$T_2 = \frac{1}{2} M \dot{y}^2 \tag{16}$$

Since we assume that the motion of the blade is sinusodial with respect to time we have the following relations

$$\dot{Y}(X) = \omega Y(X) \tag{17}$$

and

$$\dot{y} = \omega y \tag{18}$$

where ω is the fundamental natural frequency of flexural vibration.

Substituting Equations 17 and 18 into Equations 15 and 16, respectively, and then equating T_1 and T_2, we have

$$M = \int_0^L \bar{Y}(X)^2 \rho(X)\, dX \tag{19}$$

where

$$\bar{Y}(X) = \frac{Y(X)}{y} \tag{20}$$

and Y(X) is the static deflection curve. The use of the static deflection as the mode shape in the dynamic case is recognized only as an approximation. Regarding the density distribution $\rho(X)$, we again consider two cases here.

Case (1)

$$\rho = \rho_0 = \text{Constant}, \quad \rho_0 = M_b/L$$

Case (2)

$$\rho = \rho_0 \left(1 - \frac{X}{L}\right)^{1/4}, \quad \rho_0 = \frac{5}{4} \frac{M_b}{L}$$

The first case closely describes an idealized density distribution of graphite-epoxy and titanium blades while the second case is an approximation for stainless steel and boron-aluminum blades. In making the idealizations for each case, we should make sure that the integration $\int_0^L \rho\,(X)\,dX$ is close to the total mass of the blade. Figure 4(b) shows ρ as a function of x for both cases. We now evaluate the effective mass M as a function of x for each case separately.

In the first case we use the static deflection curve Y(X) as given in Equation 7 which corresponds to the deflection curve of a uniform cantilever beam under a concentrated load at x. Substituting Equation 7 into Equation 19 and carrying out the integration, we obtain

$$M = \frac{x}{L}\left[\frac{33}{140} + \frac{1}{4}\left(\frac{L}{x} - 1\right)\left(1 + 3\frac{L^2}{x^2}\right)\right] M_b \qquad (21)$$

where M_b represents the total mass of the blade. Equation 21 is plotted as a function of $\frac{X}{L}$ in Figure 6.

In the case where $\rho = \rho_0 (1 \frac{x}{L})^{1/4}$ we may use the deflection curve given in Equations 10 and 14. Since integration of Equation 19 is extremely tedious when Equations 10 and 14 are substituted, we instead use Equation 10 over the entire interval from 0 to L. The expression for the effective mass is then given by

$$M = \rho_0\, a^2 \left(\frac{L}{x}\right)^4 \int_0^L \left(1 - \frac{X}{L}\right)^{1/4} \left[\frac{X}{L}\left(\frac{2L}{x} - 1\right) + \left(2\frac{L}{x} - \frac{X}{x} - 1\right) \ell n \left(1 - \frac{X}{L}\right)\right]^2 \phi x,$$

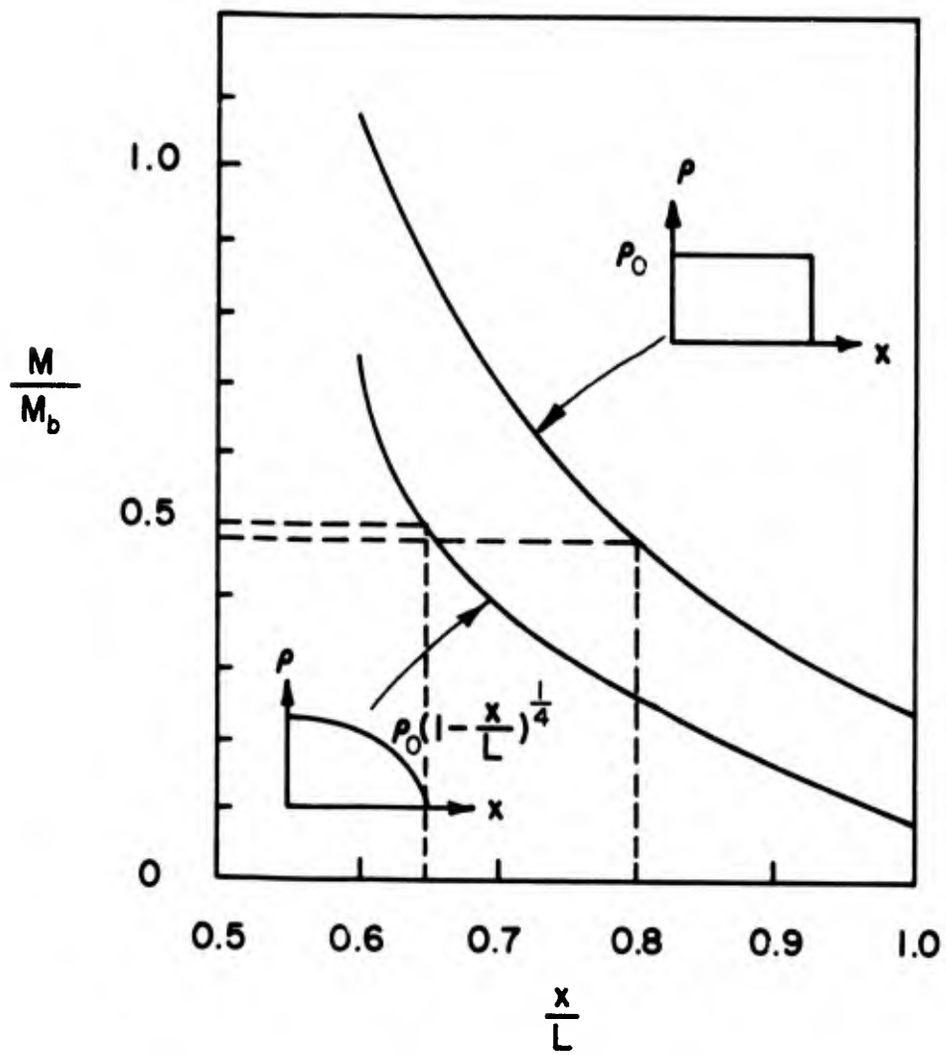

Figure 6. Effective Flexural Mass versus Location of Impact

or

$$M = \rho_0 L \alpha^2 \left(\frac{L}{x}\right)^4 \int_0^1 \bar{x}^{1/4}\left[(1-\bar{x})^2\left(\frac{2L}{x}-1\right)^2 + 2\left(1-\bar{x}\right)\left(\frac{2L}{x}-1\right)\left(\frac{L}{x}\left(1+\bar{x}\right)-1\right)\ell n\,\bar{x} + \left(\frac{L}{x}\left(1+\bar{x}\right)-1\right)^2\left(\ell n\,\bar{x}\right)^2\right] d\bar{x} \tag{22}$$

where the substitution $\bar{X} = 1 - \frac{X}{L}$ has been made for convenience. The integration in Equation 22 can be carried out with the help of the following formula

$$\int z^m (\ell n\, z)^n dz = \frac{z^{m+1}(\ell n\, z)^n}{m+1} - \frac{n}{m+1}\int z^m (\ell n\, z)^{n-1} dz \tag{23}$$

$$(m, n \neq -1)$$

Using Equation 23 in conjunction with Equation 22 we obtain

$$M = \alpha^2 \left(\frac{L}{x}\right)^4 \left[\frac{128}{585}\left(\frac{2L}{x}-1\right)^2 + \frac{128}{125}\left(\frac{L}{x}-1\right)^2 + \frac{256}{729}\frac{L}{x}\left(\frac{L}{x}-1\right) + \frac{128}{2197}\left(\frac{L}{x}\right)^2 + \frac{32}{169}\frac{L}{x}\left(\frac{2L}{x}-1\right) - \frac{32}{25}\left(\frac{L}{x}-1\right)\left(\frac{2L}{x}-1\right) - \frac{32}{81}\left(\frac{2L}{x}-1\right)\right] M_b \tag{24}$$

Equation 24 is plotted in Figure 6. This figure shows that the effective mass of the mass-spring system increases as the location of impact is closer to the root of the blade as previously shown in Figure 5 for the stiffness k.

3. NATURAL FREQUENCIES AND INITIAL CONDITIONS OF THE MASS-SPRING SYSTEM

a. Initial Velocity Only

When the mass-spring system is given an initial velocity alone by the impact of the foreign object, the sinusoidal motion can be described as shown in Figure 7(a).

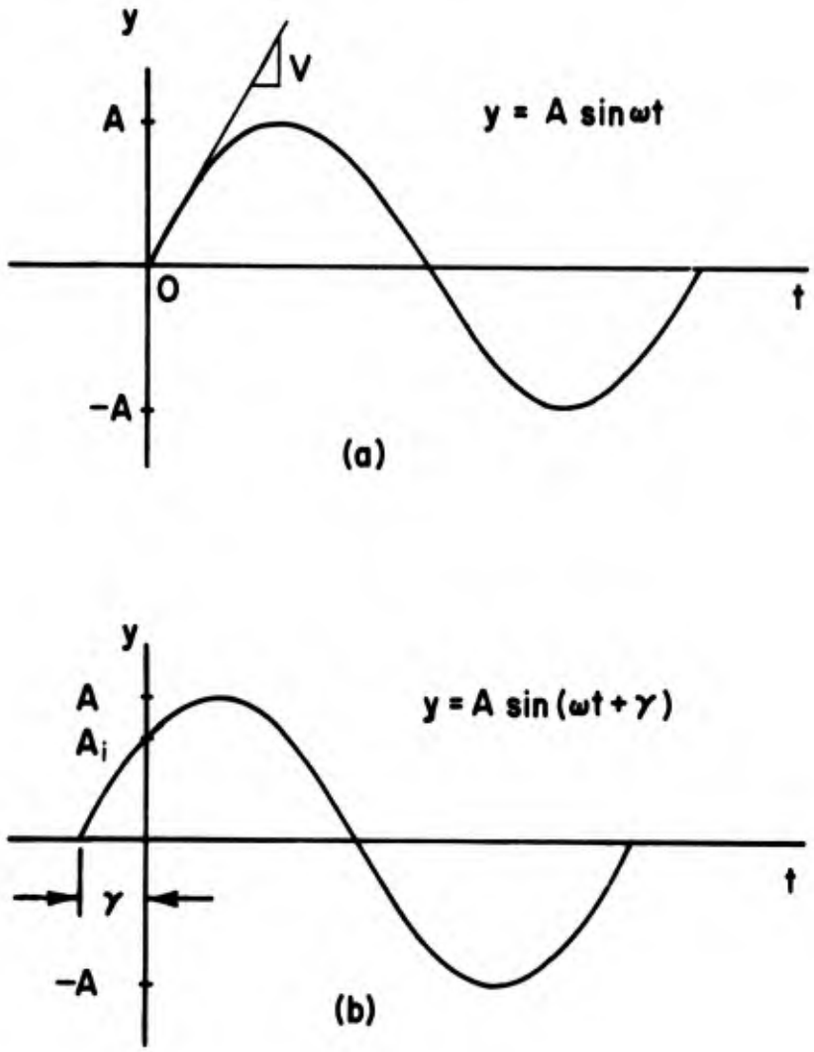

Figure 7. Resulting Vibration: (a) Without Initial Displacement; (b) With Initial Displacement

The maximum velocity, V, occurs at t = 0 and the maximum displacement, A, occurs at $t = \frac{\pi}{2\omega}$ where ω is the natural frequency of the mass-spring system. For sinusoidal motion we have the following relations

$$y = A \sin \omega t$$

$$\dot{y} = V \cos \omega t \tag{25}$$

From Equation 25 we recognize that

$$A = \frac{V}{\omega} \tag{26}$$

For a conservative system, the maximum potential energy must be equal to the maximum kinetic energy, i.e.,

$$\frac{1}{2} k A^2 = \frac{1}{2} M V^2 \tag{27}$$

Substituting Equation 26 into Equation 27 we obtain the well-known relation

$$\omega = \sqrt{\frac{k}{M}} \tag{28}$$

From Equations 9, 13, 21 and 24 it appears that ω also depends upon the location of impact. The natural frequency ω is plotted as a function $\frac{X}{L}$ in Figure 8 for the two cases considered before:

(1) I = Constant, ρ = Constant;

(2) $I = I_o \left(1 - \frac{X}{L}\right)^2$, $\rho = \rho_o \left(1 - \frac{X}{L}\right)^{1/4}$

Figure 8 shows that ω is practically independent of $\frac{X}{L}$. Since, physically, the natural frequency depends upon the material and geometry of the blade, it should be independent of the location of impact. For a continuous beam, impact at different points along the beam may excite different modes of vibration. However, based upon experimental results,

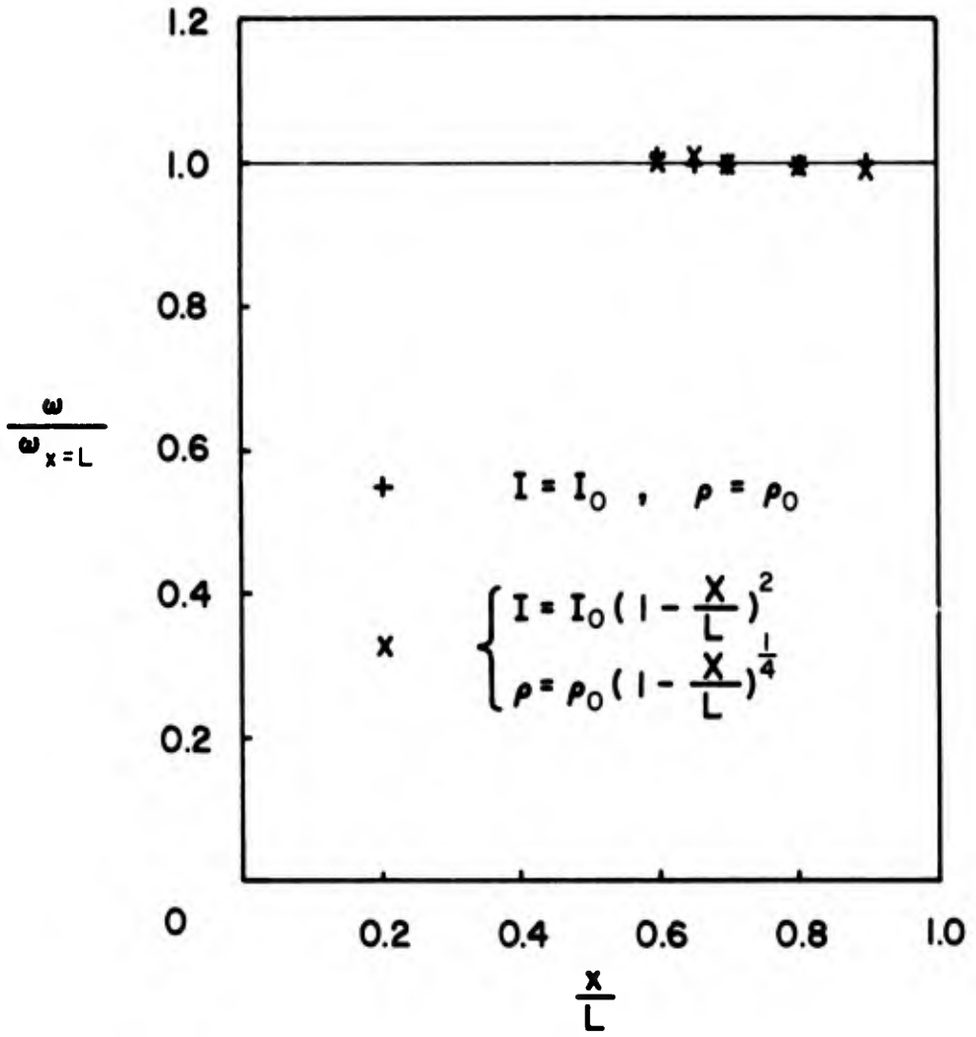

Figure 8. Natural Frequency (Flexural) versus Location of Impact

the vibration of the beam essentially corresponds to that of the fundamental mode when the point of impact falls within the range $0.6 \leq \frac{x}{L} \leq 0.85$.

The initial velocity V of the system can be determined from the principle of conservation of linear momentum and the definition of the coefficient of restitution. The principle of conservation of linear momentum states that when the sum of the impulses of the external forces acting on a system of particles is zero, the total momentum of the system remains constant. For a nonrotating blade, the sum of the total momentum before impact is mv_n and after impact is $mv_n' + MV$, Figure 3. Thus, we have

$$mv_n = mv_n' + MV \tag{29}$$

where v_n and v_n' are the normal velocities of the foreign object before and after impact, respectively. The coefficient of restitution e is the ratio of the relative velocity of the two particles after impact to the relative velocity of the two particles before impact, i.e.,

$$e = \frac{\Delta v_{\text{after impact}}}{\Delta v_{\text{before impact}}} = \frac{V - v_n'}{v_n} \tag{30}$$

The values of e are always between 0 and 1 and depend to a large extent on the two materials involved. However, it also varies considerably with the impact velocity and the shape and size of the colliding bodies. The relationship between e and the impact velocity is obtained experimentally. A detailed discussion of the coefficient of restitution e is given in Appendix I.

From Equations 29 and 30 we can express V in terms of v_n through the elimination of v_n'.

$$V = \frac{m(1 + e)}{M + m} v_n \tag{31}$$

For normal impact we have $v = v_n$. If the direction of v is not parallel to the normal direction of the blade at the point of impact, then we have

$$v_n = v \sin\theta \tag{32}$$

where θ is the incident angle defined in Figure 3.

After having determined V, we can determine A (the maximum deflection of the lumped mass) from Equation 26. The maximum deflection δ of the blade at the tip can then be calculated from the static deflection curve (Equation 8 or Equation 14) by replacing y by A. The maximum flexural stress which occurs at the root of the blade can be obtained from the formula

$$\sigma_{max} = \frac{kAxh}{2I_o} \tag{33}$$

where h is the thickness of the blade cross-section at the root. All the quantities discussed in this section were evaluated for several B/Al and Gr/Ep beams of uniform cross-section and are listed in Table 1.

b. Initial Velocity and Initial Displacement

If the motion of the mass-spring system is considered to start with an initial displacement A_i as well as an initial velocity, the equation of motion of the system can be written as

$$y = A \sin(\omega t + \gamma) \tag{34}$$

where γ is the phase angle which is related to the initial displacement A_i by the following relation

$$\gamma = \sin^{-1} \frac{A_i}{A} \tag{35}$$

Substituting Equation 35 into Equation 34, we have

$$y = A \sin(\omega t + \sin^{-1} \frac{A_i}{A}) \tag{36}$$

TABLE 1

THEORETICAL AND EXPERIMENTAL RESULTS FOR THE CASE WITHOUT INITIAL DISPLACEMENT
(B/Al and Gr/Ep)

Beam Matl	V, ft/sec		ω, Hz		A, in		δ, in		σ_{max} ksi
	Theo	Exp	Theo	Exp	Theo	Exp	Theo	Exp	
B/Al	62	58	244	241	.48	.51	.66	--	130
	63.5	67.1	244	217	.488	.453	.58	.57	115
	64.0	33.5	244	226	.492	.495	.585	.649	126
	68.5	83.2	244	222	.525	.577	.625	.710	147
	87.5	91.8	244	197	.670	.829	.800	.910	211
	94.5	90.8	244	214	.730	.848	.870	1.00	216
	111.4	146.8	244	195	.855	.917	1.02	1.091	233
	121.6	121.3	244	234	.933	.831	1.11	1.068	211
	124.9	63.6	244	208	.958	.876	1.14	1.045	223
	125.9	146.2	244	293	.966	1.151	1.14	1.35	293
B/Al	132.2	134.4	244	--	1.014	1.092	1.201	1.290	278
Gr/Ep	33.6	33.9	190	133	.375	.566	.515	.699	108
	47.6	47.2	190	145	.660	.751	.910	.863	143
Gr/Ep	64.8	106.5	190	123	.885	.831	1.21	.964	158

A plot of Equation 34 is shown graphically in Figure 7(b). The velocity of the mass-spring system is then given by

$$\dot{y} = \omega A \cos\left(\omega t + \sin^{-1} \frac{A_i}{A}\right) \tag{37}$$

and the initial velocity V is obtained as

$$V = \omega A \cos \sin^{-1} \frac{A_i}{A} \tag{38}$$

It is observed that as A_i tends to 0, Equation 38 coincides with Equation 26.

Equation 38 can be solved for A by trial and error. The influence of A_i, in general, is to increase the damage to the blade for a given bird velocity. It is very easy to verify from Equations 38 and 31 that in order to produce the same deflection A the following relationship between v and A_i exists, i.e.,

$$\frac{[v]_{A_i \neq 0}}{[v]_{A_i = 0}} = \left[\cos \sin^{-1} \frac{A_i}{A}\right] \frac{[1+e]_{A_i = 0}}{[1+e]_{A_i \neq 0}} \tag{39}$$

Numerical results obtained for this case are listed in Table 2.

TABLE 2

THEORETICAL AND EXPERIMENTAL RESULTS FOR THE CASE WITH INITIAL DISPLACEMENT (B/A1)

x in	W* H_2	v ft/sec	A_i in	V* in/sec	A, in		δ, in	
					Theo	Exp	Theo	Exp
3.2	151	296	0.4	900	1.13	0.75	1.42	1.30
	151	337	0.4	1020	1.20	0.80	1.55	1.41
	151	367	0.4	1110	1.27	0.90	1.63	1.57

REMARKS:

* Experimental data

$\rho_o = 1.692 \times 10^{-3}$ lb/in, L = 4 in, b = 0.4 in, h = 0.045 in.

SECTION III

EXPERIMENTAL PROCEDURE AND RESULTS

Laboratory experiments to test the "Lumped Parameter" theory were designed and conducted in the AFML-LLN High Velocity Impact Physics facility. It was decided that the complex geometry of the blade would be idealized for purposes of these tests to a simply clamped cantilever beam. It was determined that a cantilever beam geometry was a legitimate test to check the applicability of the theory without incurring the expense in time and money to obtain either full scale or reduced scale models of actual blade geometries. The simple-geometry laboratory size cantilever beam samples are sufficiently inexpensive to allow testing of a variety of different materials and composite layup configurations.

The several motion parameters resulting from soft body (bird) impact on the beam that are to be monitored include the following (Figure 2):

(a) Mass of projectile, m
(b) Velocity of projectile, v
(c) Velocity of projectile at beam failure, v_m
(d) Location of impact, x
(e) Deflection of beam as function of X, Y(X)
(f) Initial velocity of beam after impact, V
(g) Maximum tip deflection, δ
(h) Maximum tip deflection at beam failure, δ_m
(i) Frequency of flexural vibration, ω
(j) Thickness, width, and length of beam, h, b, L
(k) Longitudinal Young's modulus and strength of beam, E and σ_m

In addition there are other parameters of interest. For example, contact time of the rubber projectile on the beam, higher bending modes and torsional frequencies were measured on occasion. The techniques required to determine this many parameters on a single impact become rather sophisticated. An attempt was made to have redundant measurements on all important parameters to ensure no loss of data and to provide internal checks.

1. EXPERIMENTAL PROCEDURE

The beam dimensions were fixed as nearly as possible. Occasionally slight differences occurred when an effort was made to obtain a maximum number of test samples with minimum waste from a single piece of material. The samples were 4 1/2 inches long to allow 1/2 inch in the clamp and 4 inches of free beam. The samples were cut 0.4 inch wide. The beam thickness varied with the material, the number of plies, the ply layup, and the manufacturing technique. The thickness varied from 0.035" to 0.066". The exact dimensions of each sample were measured and used in the analysis.

The materials chosen for the tests were one metal and two composites. The composites each had variations in them making nine different kinds of samples to use to test the theory.

The projectile used to impact the sample was a cylinder .295" diameter by .295" long of RTV-11 silicone rubber made by General Electric. The cured cylinder has a mass of 350 milligrams. The RTV rubber was chosen because it was a convenient, easy to handle material that has been shown in other experiments to behave in a manner similar to bird flesh upon impact. Figure 9 on RTV shows projectile in the sabot. The sabot is a plastic bore fitting carrier that protects the projectile from the launch tube walls. The sabot is either stopped in the launch tube or deflected away so as not to interfere with the experiment.

The projectile is launched from an 0.50 caliber launch tube and is propelled by either air or burning powder. The smooth bore tube will accept adapters either for the compressed air breech (Figure 10) or a breech (Figure 11) containing a rifle shell with gun powder. The muzzle end of the launch tube is also adaptable. It will accept fixtures to stop the sabot on low velocity shots or to retard and deflect the sabot out of the flight path on the higher velocity shots. Figure 12 shows the deflection assembly. The split launch tube allows the propellant gases to escape while the sabot is being slowed by friction. The projectile separates from the sabot and flies free exiting the launch tube.

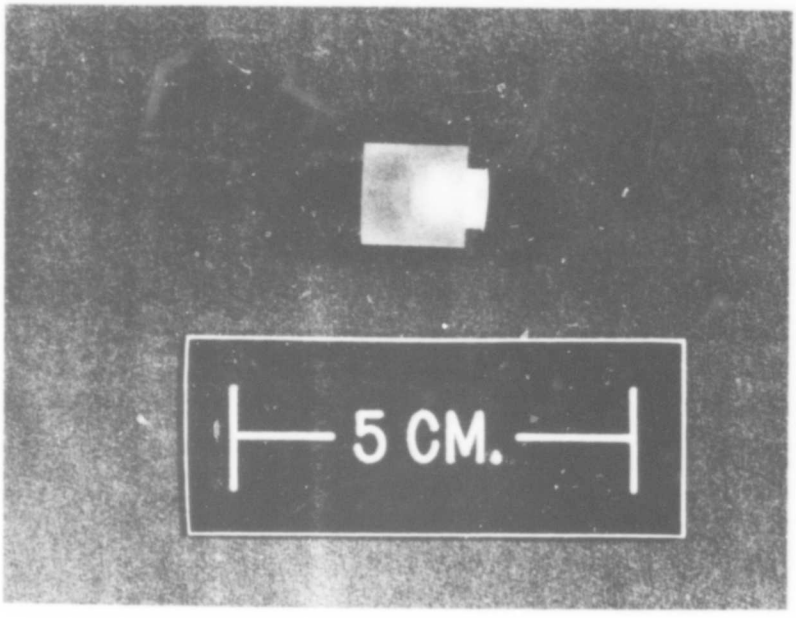

Figure 9. RTV Rubber Projectile in Sabot

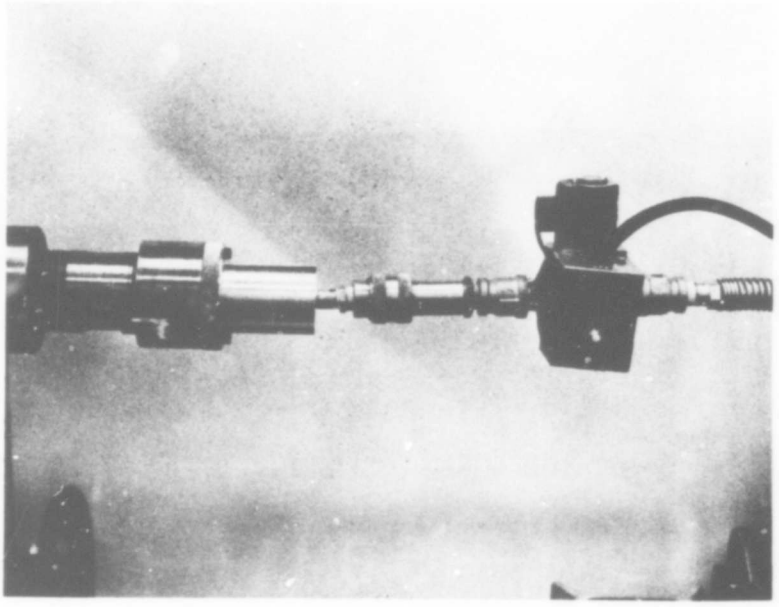

Figure 10. Compressed Air Breech

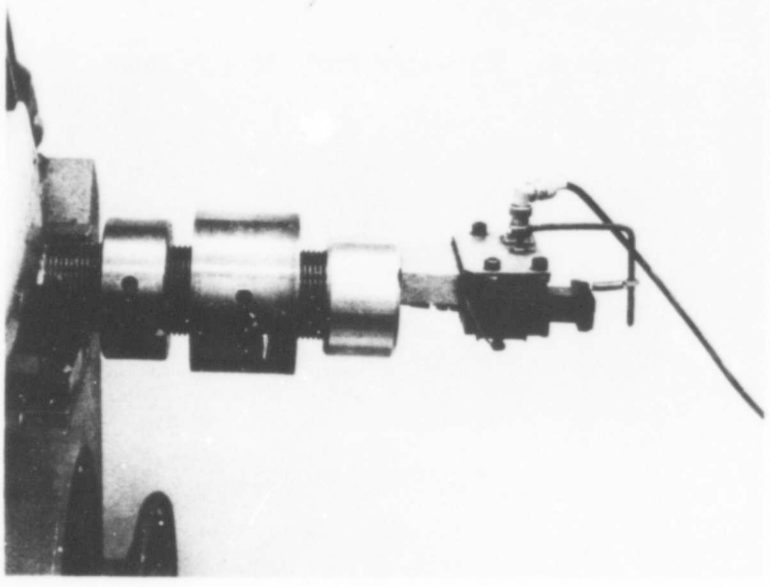

Figure 11. Powder Breech

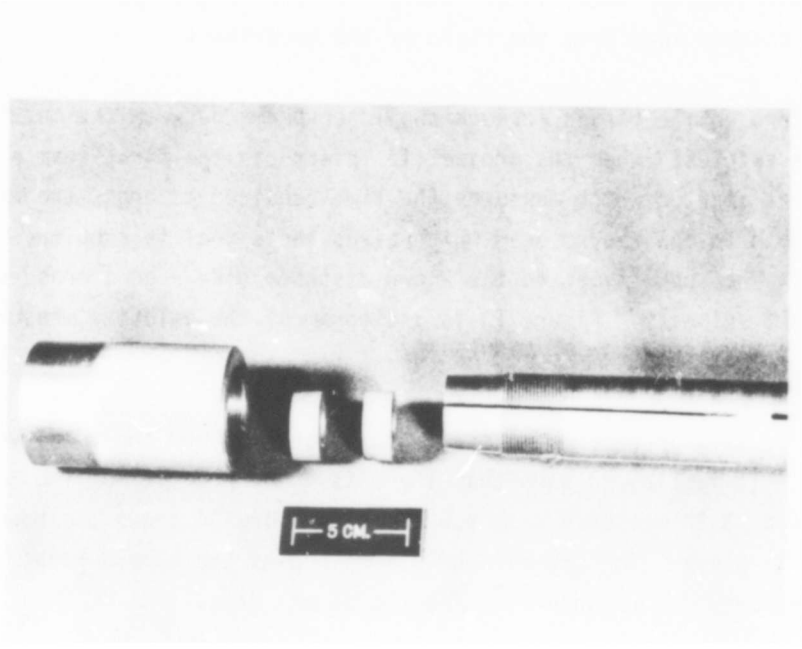

Figure 12. Sabot Stripper

The larger diameter sabot is deflected from the flight path and into a waiting catcher away from the field of the experiment.

The projectile passes through two laser beams between the muzzle and the test samples. When the projectile interrupts the first beam a counter is started which measures the time required to cross the known path length to the second beam which gives the signal to stop the counter. The known time and the known distance give a good measure of the impact velocity. Figure 13 is a diagram of the velocity measuring unit.

The cantilever beam is mounted a few inches beyond the final velocity station. It is clamped such that there is 4" of free beam. The impact point is at 3.2" measured from the clamp. Figure 14 shows the beam mounted in place. The engraved grid seen behind the sample gives fiducial marks for reducing the framing camera data.

Dynafax framing camera -326 capable of taking 224 pictures at rates up to 26,000 frames per second is shown in Figure 15. It is a continuous access type camera; hence the light duration must be tailored to initiate during the event and extinguish in time to prevent rewrite. The camera is used in a shadowgraph mode with the flash lamp behind the impact event. The camera is focused on the whole beam with enough depth of field to see both the beam and the grid.

Taking advantage of the framing camera light through a beam splitter arrangement the streak camera is used to measure very accurately the motion of the impacted beam at a point at or just above the point of impact. The streak camera used (Figure 16) is a Beckman and Whitley Dynafax Streak Camera Model 319B. The streak camera is ideally suited to accurately measure the velocity of short duration movement. A side benefit is the ability of the streak camera to register to torsional mode vibrations.

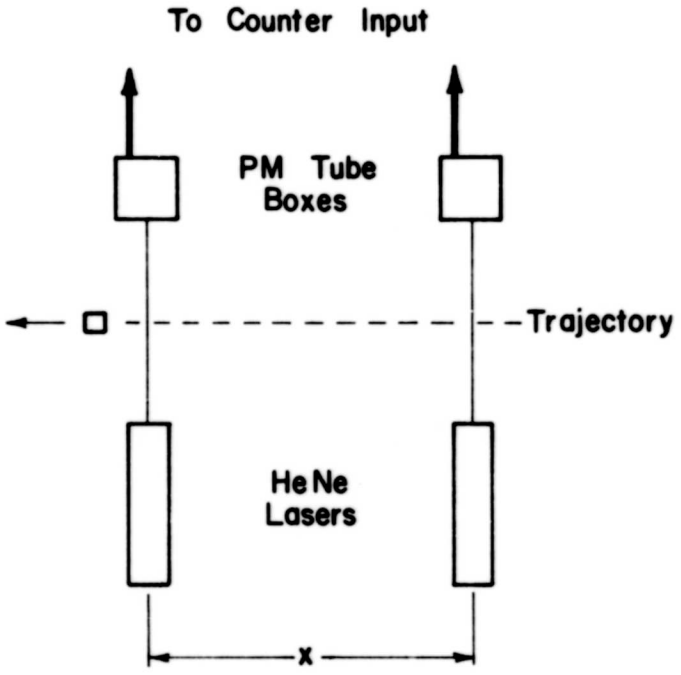

Figure 13. Velocity Measuring Unit

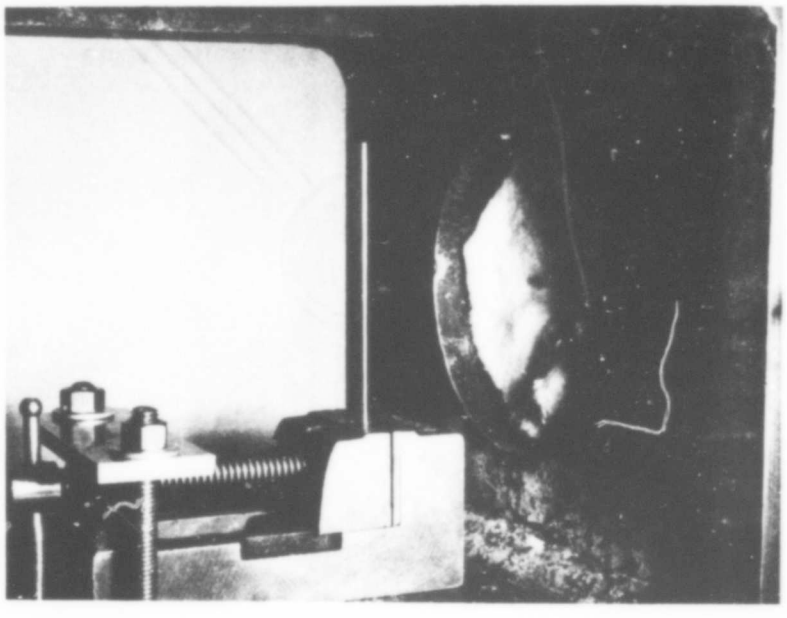

Figure 14. Cantilever Beam Mounted in Tank

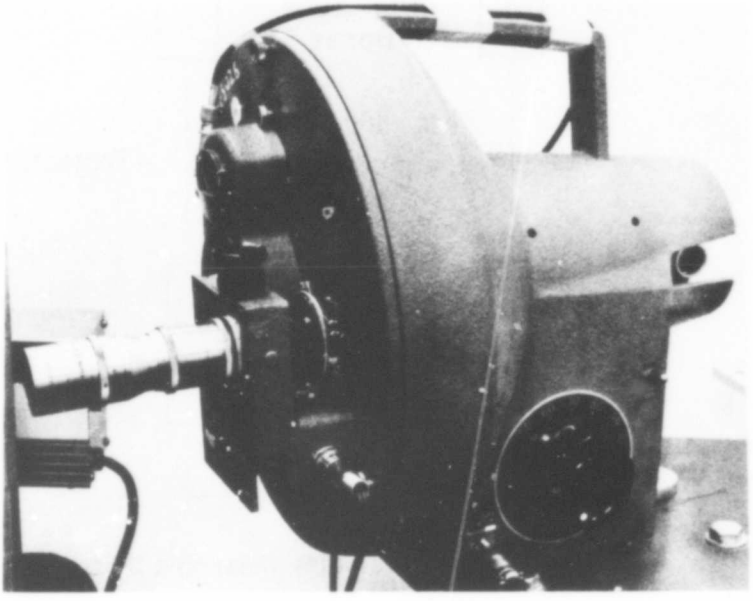

Figure 15. B & W Model 326 Framing Camera

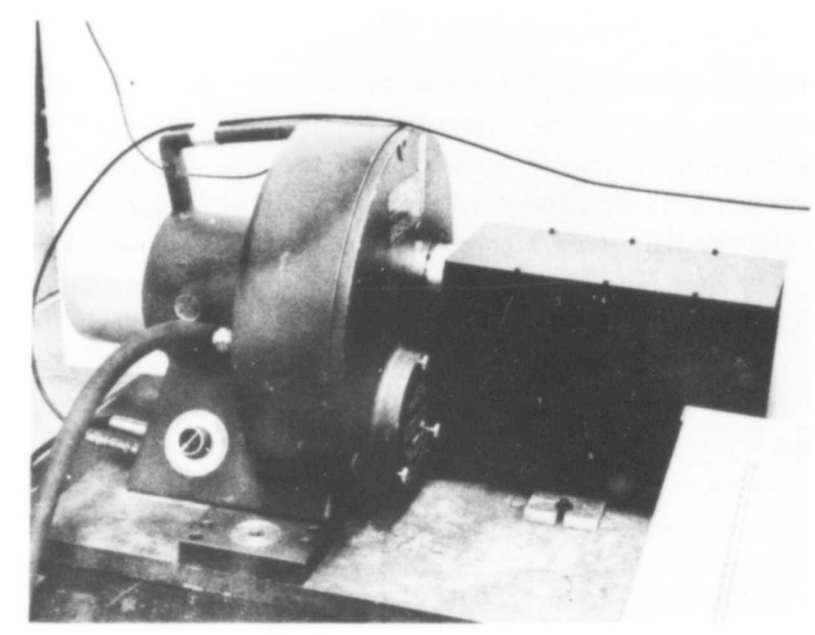

Figure 16. B & W Model 319B Streak Camera

Strain gauges are glued to the beam on both sides as shown in Figure 17 and are connected to a strain gauge bridge with the proper amplifiers to measure the absolute strain and the variation of strain with time at a point on the beam near the clamp.

The incoming velocity v is measured by the laser velocity stations and, when needed, by the streak camera. The initial velocity of the beam V was measured by the streak camera and the framing camera. The flexural frequency is measured most accurately by the strain gauges but also from the framing camera records. The various desired deflection (displacement) measurements are taken from the framing camera pictures (Figure 18) and the streak camera record. The angle at maximum displacement and at break off can only be measured on the framing camera pictures. Torsional frequencies are most accurately measured from the streak record (Figure 19) though they can be seen as second order vibrations on the strain gauge records. Higher flexural mode frequencies, when they are excited, can also be seen on the strain gauge (Figure 20) records. Figure 20 also shows slow damping of the first flexural mode following higher mode bending on first cycle. The several internal consistency checks on the data gathered increase the confidence of the measurements made.

2. EXPERIMENTAL RESULTS

The maximum tip deflection δ_m of the cantilever beam when impacted at the velocity v_m that will just cause root failure can not be measured directly because at that velocity the beam initiates a mode of vibration that is more like free-hinged vibration than simple harmonic motion of a disturbed cantilever beam. As a result, it is difficult to measure the maximum deflection of the beam just at the break off velocity. However, the lumped parameter model calls for the deflection at break off velocity as one of the parameters, so an alternate method of determining the maximum deflection at v_m was devised.

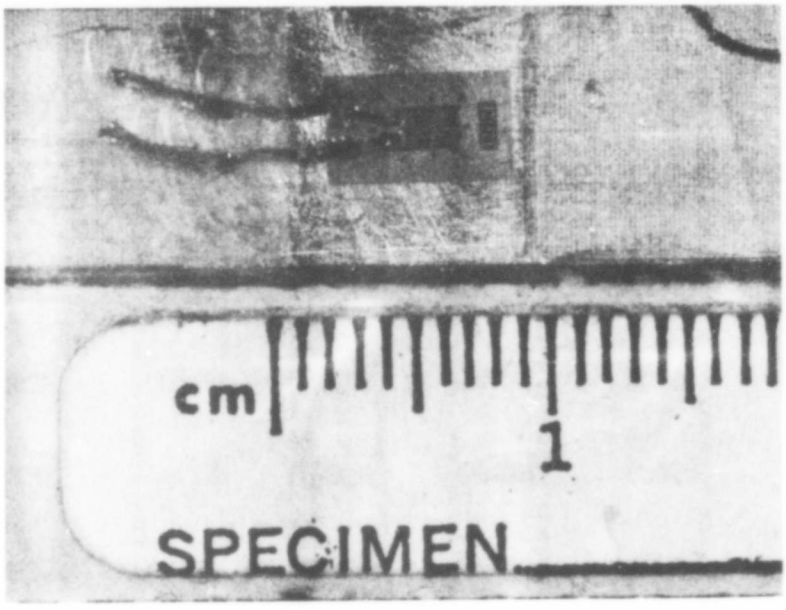

Figure 17. Strain Gauges on Beam

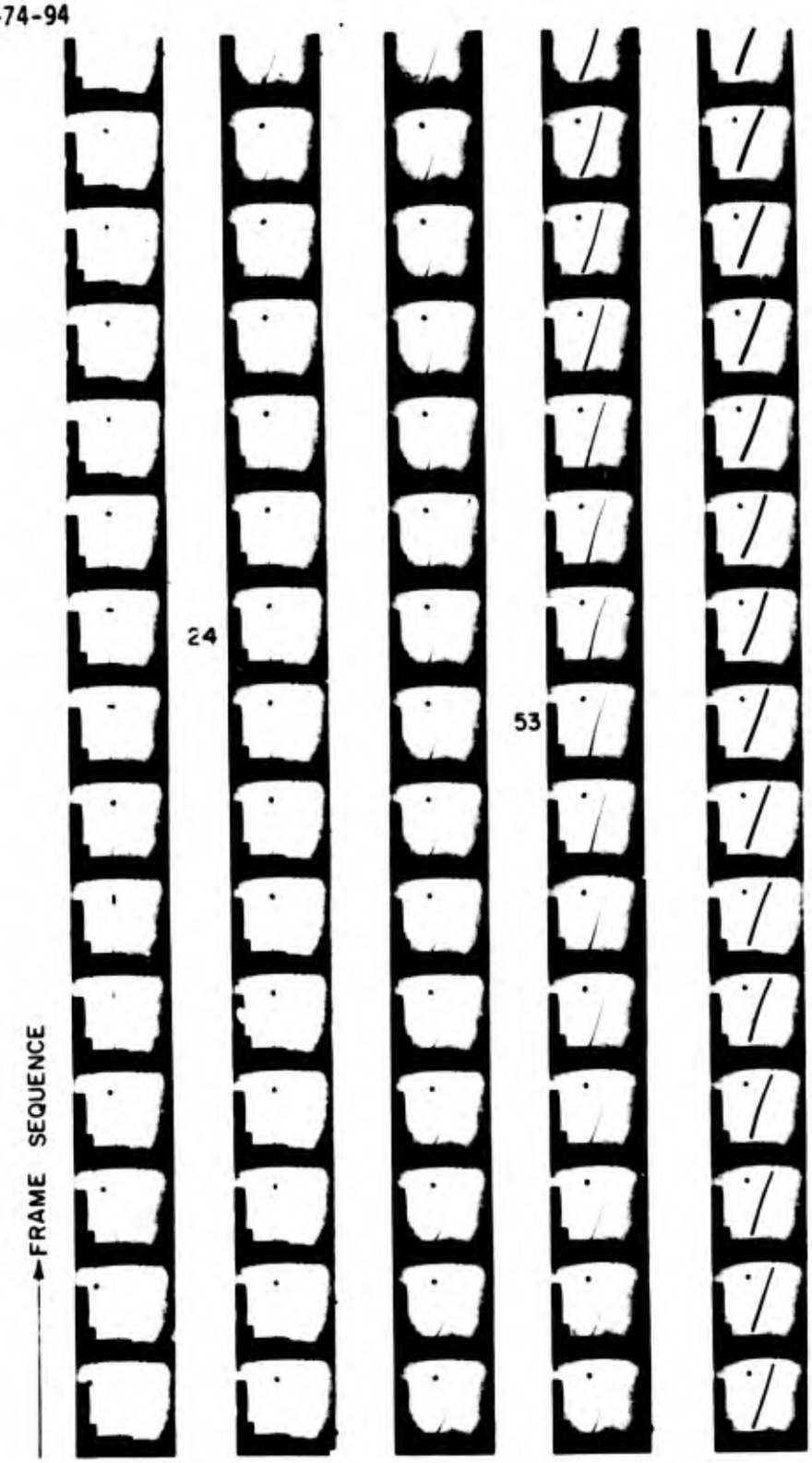

Figure 18. Impact RTV Slug on B/Al Beam - Framing Camera Record (Impact Velocity = 333 ft/sec, Camera Speed = 21360 frames/sec)

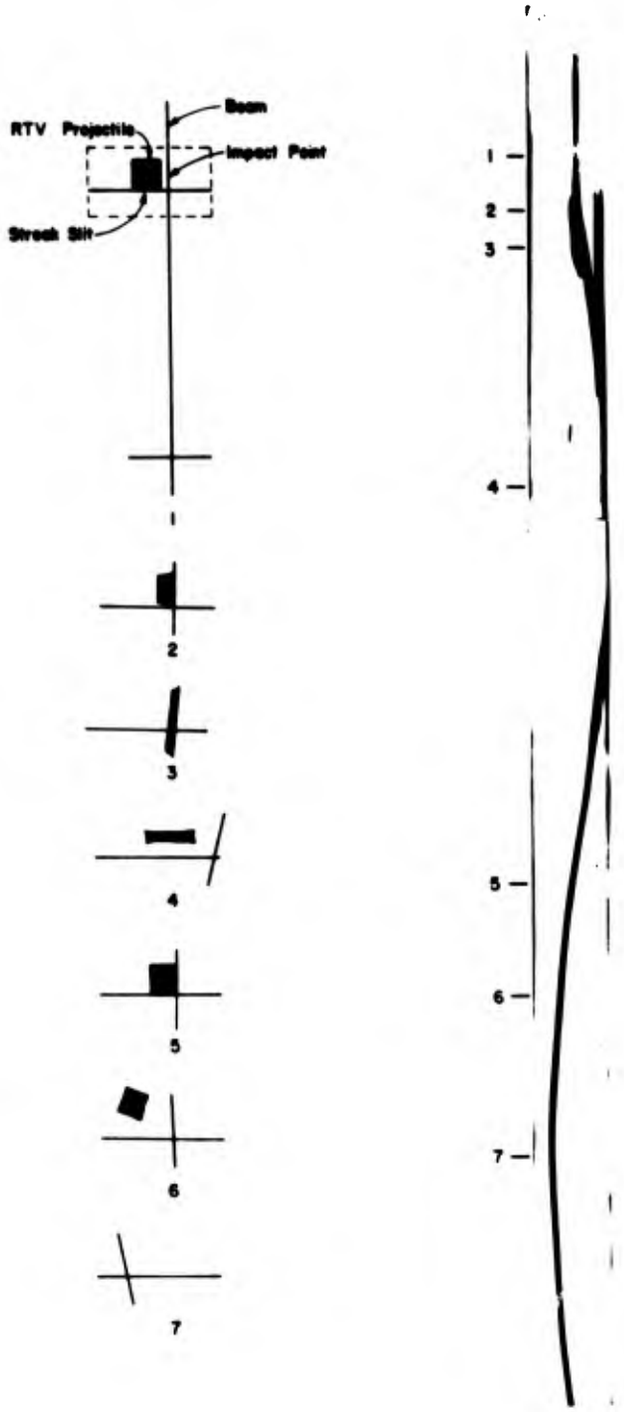

Figure 19. Streak Camera Record

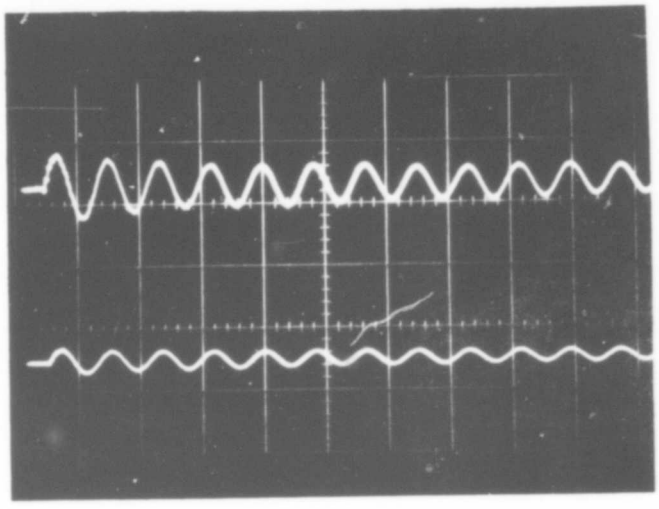

⟶ t, 5msec/cm

Figure 20. Strain Gauge Record for Shot 6713 (B/Al) with SS Mesh

The impact velocity that just breaks the beam at the root 50% of the time is determined by plotting all the test results for, e.g., B/Al beams as shown in Figure 21. The velocity v_m for a given material and geometry can be seen rather easily. Next the maximum deflection δ as measured from the framing camera pictures is plotted versus v as shown in Figure 22. A best fit curve is drawn through these points and the intersection of the curve with the vertical v_m line is taken to be the deflection δ_m or the deflection at break off velocity.

Next, a single plot of the beam deflection data for all materials is of interest. Here deflection is measured at the point of impact. Since the mass of each material type is different, a normalized plot is required. In the analytical section of this report, the following momentum transfer equation was developed:

$$V = \frac{M(1+e)}{(m+M)} \quad v \tag{31R}$$

In terms of deflections Equation 31R becomes:

$$A = \frac{V}{\omega} = \frac{m(1+e)}{\omega(m+M)} \quad V \tag{40}$$

Similar equations may be written for the deflection corresponding to the threshold velocity v_m for breaking the beam at the root. By dividing the equation describing deflection at any velocity by the equation for maximum deflection (at break off) a normalized relationship may be written:

$$\frac{A}{A_m} = \frac{(1+e)}{(1+e_m)} \quad \frac{v}{v_m} \tag{41}$$

This equation states that by knowing the coefficient of restitution as a function of velocity and the maximum deflection and velocity, A_m and v_m, for a given material, the deflection at any velocity may be predicted.

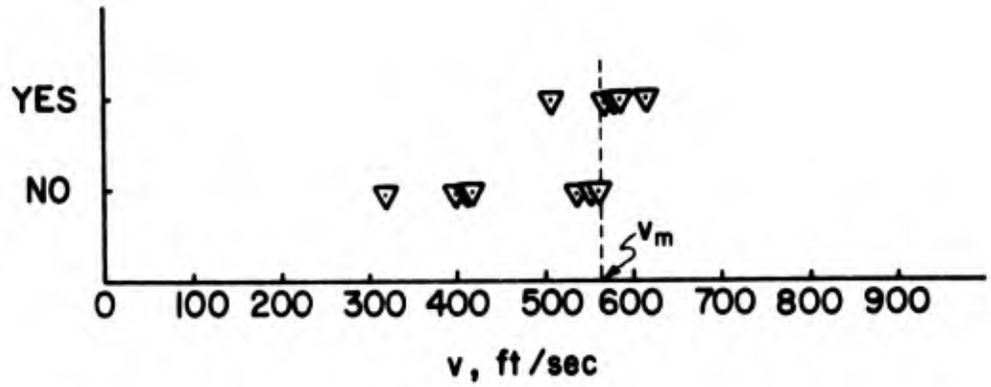

Figure 21. Root Failure versus Impact Velocity (B/Al)

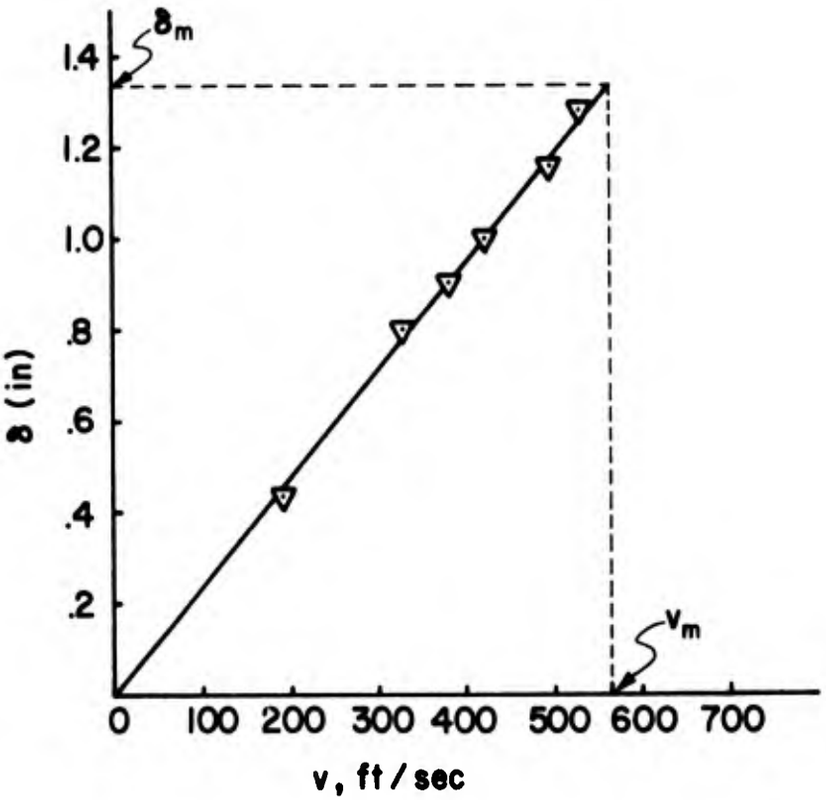

Figure 22. Maximum Tip Deflection versus Impact Velocity (B/Al, 0.058" Thick)

Figure 23 displays the normalized deflection for all materials tested in this effort. As can be seen, the data fit the prediction quite well and evenly scattered about the line. The line is curved by virtue of the variation in coefficient of restitution with velocity (described in Appendix I). It is worthwhile to note that the data for the pre-deflected beams also fit the prediction when the initial displacement is taken into account.

Other results obtained (e.g., natural frequencies and initial velocities) are listed in Tables 1 and 2. Also reported in Table 3 are the results for torsional vibration. The analysis for this case is described in Appendix II.

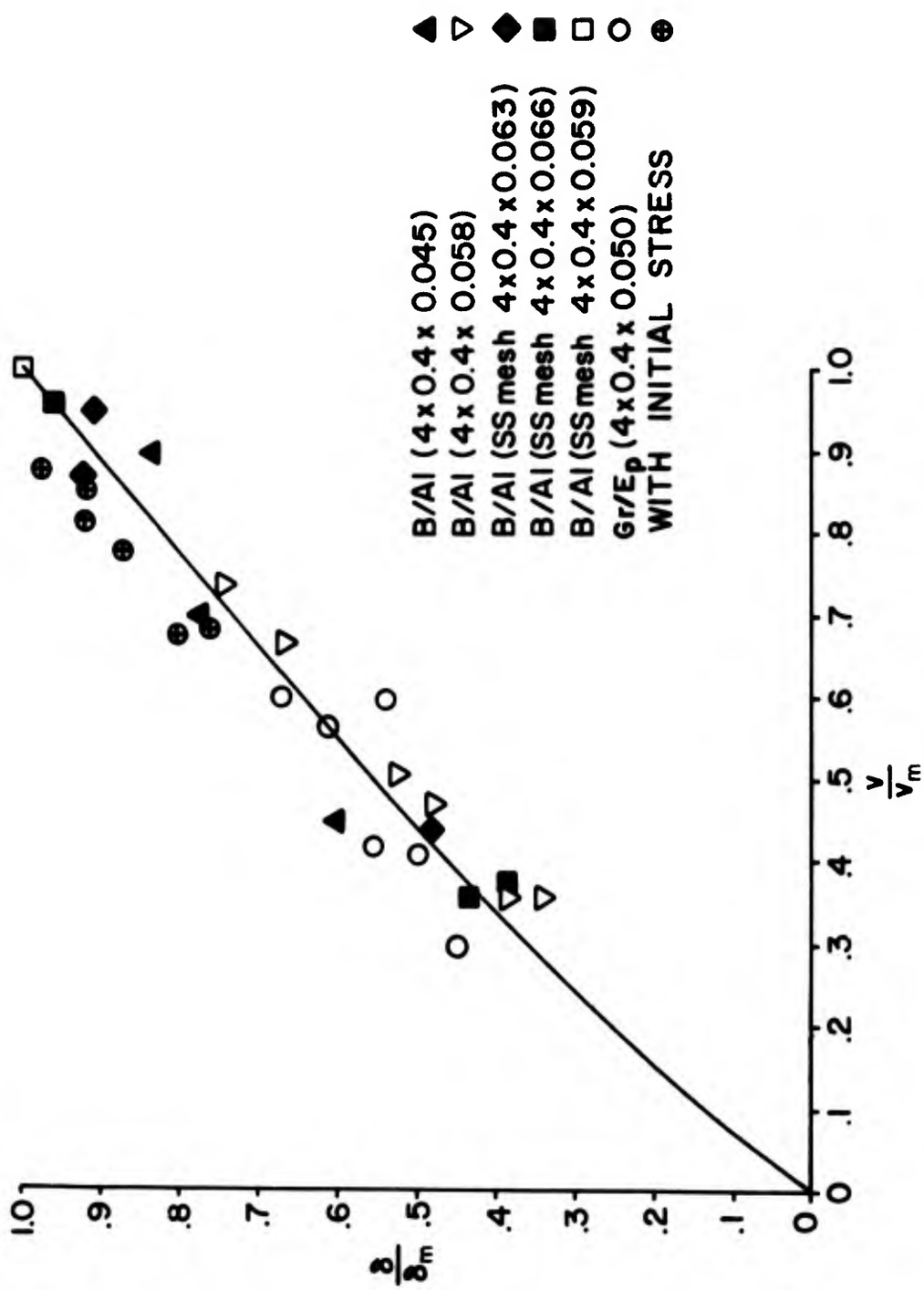

Figure 23. Maximum Deflection at Point of Impact versus Impact Velocity

TABLE 3

IMPACT VELOCITY, MAXIMUM DEFLECTION, AND COEFFICIENT OF RESTITUTION AT FAILURE

Target Material	v_m (ft/sec)	A_m (in)	e_m	Symbol
B/Al (4x0.4x0.045)	425	2.10	0.32	
B/Al (4x0.4x0.058)	565	1.36	0.275	
B/Al (SS mesh - 4x0.4x0.063)	590	1.18	0.270	
B/Al (SS mesh - 4x0.4x0.066)	580	1.05	0.270	
B/Al (SS mesh - 4x0.4x0.059)	550	1.14	0.280	
Gr/Ep (4x0.4x0.050)	290	1.56	0.39	

Remarks:

Refer to Figure 23.

SECTION IV

DISCUSSION OF EXPERIMENTAL RESULTS

As seen in Tables 1, 2 and 4, the lumped parameter model reasonably predicts the first mode bending frequency, first mode torsional frequency, maximum deflection and initial velocity of a simple uniform cantilever beam struck at by a soft projectile. Detailed photographic and strain gauge analysis reveals that even though the beam is struck at the center of percussion, higher modes of bending are induced but that these quickly dampen and are nonexistent by the end of the first cycle of motion. A typical strain gage record of this motion is shown in Figure 20. Figure 24 displays the high speed photographs of the impact of an RTV projectile against a B/Al beam (4 in x 0.4 in x 0.045 in) at a velocity of 392 ft/sec. This impact velocity is only 28 ft/sec below that required for breakage of the beam at the root. The framing rate is 21265 frames/sec and only every other frame is printed here. The projectile in the lower left corner frame (frame sequence proceeding upwards) enters from the left and impact the beam, undergoes severe compression, relaxes and remains nearly stationary. The disturbance is seen to move to the beam root in the first few frames and the beam undergoes both first and higher mode bending until maximum deflection occurs. The higher modes dampen and the beam undergoes damped simple harmonic oscillation until it comes to rest.

At impact velocities where the beam fails at the root the lumped parameter analysis is inapplicable as new phenomena occur. Figure 18 displays this motion very well. The conditions are the same as for Figure 24 but here the impact velocity is 333 ft/sec, and the camera speed is 21360 frames/sec. In this a disturbance moves from the impact site to the root. At maximum deflection, the root stress is assumed to be sufficiently large that the beam plastically deforms, and, for all practical purposes, fails. A new type of oscillatory motion sets in where the root and tip act as nodal points. The beam may be described as free-hinged (FH) during this portion of the event. The bending frequency in this mode may be estimated by counting the number of frames for the

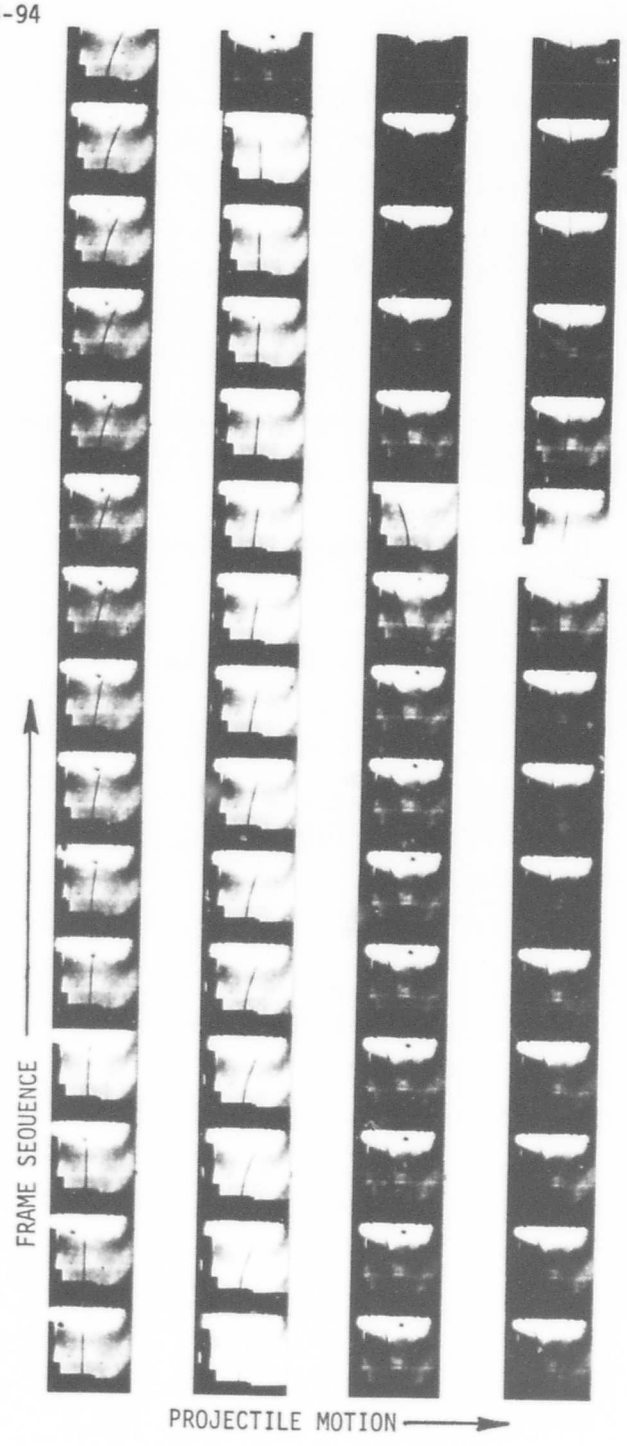

Figure 24. Impact at RTV Slug on B/Al Beam (Impact Velocity = 392 ft/sec, Camera Speed = 21265 frames/sec)

beam to oscillate a given number of cycles and dividing this number into the camera framing rate. Performing this operation on the beam shown in Figure 18 yields a frequency of 667 Hz. This motion may be predicted from beam theory,

$$f_{FH} = \frac{\omega_{FH}}{2\pi} = \frac{(3.927)^2}{2\pi}\sqrt{\frac{EI}{M_b L^3}} \qquad (42)$$

Substituting the appropriate values for this case into Equation 1 yields a value of 671 Hz.

Subsequently the beam breaks away completely from the root and undergoes what may be termed free-free (FF) oscillatory motion with the tips still acting as nodal points. Again, by observing this motion in Figure 18 the frequency of this type motion is measured as 1017 Hz. Beam theory, in this case, predicts a frequency of 975 Hz from the equation:

$$f_{FF} = \frac{\omega_{FF}}{2\pi} = \frac{(4.73)^2}{2\pi}\sqrt{\frac{EI}{M_b L^3}} \qquad (43)$$

The case just described where the two new types of motion set in at break-off velocities is typical of that observed for all composite materials evaluated in this effort.

SECTION V

CONCLUSIONS AND RECOMMENDATIONS

As the failure of turbine fan blades due to impact of foreign objects such as birds becomes more and more critical in the application of advanced composites, an exploratory study has been made in this report to develop a simple yet analytically sound model which can predict the dynamic behavior of blades. As a first step, a cantilever beam with uniform geometry and mass distribution was chosen in place of the actual blade and a soft RTV projectile was used to simulate the bird impact.

The analytical model we adopted in lieu of the cantilever is a one mass-spring system. The results seem encouraging as the following observations indicate:

1. The model predicts that the fundamental flexural frequency is almost insensitive to the location of impact as should be required (Figure 8) and the calculated frequencies compare fairly well with the experimental data.

2. The model is fairly accurate in predicting the initial velocity and maximum deflection of the cantilever beam (Tables 1 and 2 and Figure 23).

The present approach is a first order approximation to a rational analysis of the impact failure. Therefore, more detailed study is needed to fully understand and describe the phenomenon.

First, since the impact induces vibration of various modes, refined model should be allowed more degrees of freedom. This may be accomplished by adding more identical masses or by using an optimum model with fewer masses of different magnitude.

Second, it is necessary to study the momentum transfer mechanism between the bird and blade. In the present work the momentum transfer was relatively easily analyzed due to the simplicity of the projectile geometry and behavior. However, in real situations, degeneration of bird upon impact is not well understood. We need to find what are the pertinent parameters descriptive of this phenomenon.

Third, any failure analysis in not possible without a failure criterion. Although no attempt has been made here, our ultimate goal is the prediction of failure.

Finally, whereas the present work is concerned with the global damage, i.e., the root failure, the local damage is frequently observed also. Thus, depending on the situation, the problem is not only one of vibration but of wave propagation. This aspect should further be looked into.

We can say that the simple mass-spring model seems to yield a fairly accurate picture of the vibrational characteristics of a cantilever beam impacted by a rubber projectile. The model should be refined accordingly as the level of accuracy of the required information increases.

REFERENCES

1. Advanced Composites Design Guide, Vol. V, Air Force Materials Laboratory (AFML/LC), Wright-Patterson AFB, 1973.

2. B. L. Koff, "Graphite Fan Blade Development," National Aeronautic and Space Engineering and Manufacturing Meeting, Society of Automotive Engineers, September 1971.

APPENDIX I

MEASUREMENT OF THE COEFFICIENT OF RESTITUTION IN RTV

High speed photographic observation of the impact of RTV cylinders against the cantilever beams revealed that the projectiles did not remain in contact with the beam throughout the impact event. Rather, the projectile came to nearly a standstill at impact, while the beam moved away from the impact site. In some cases the projectile reversed its motion and retreated very slowly from the impact site. Thus, the assumption of a plastic impact was not valid, and an analysis based on inelastic behavior was required.

A series of experiments was conducted to measure the coefficients of restitution of RTV impacting various materials. Spheres of RTV-11 measuring 0.5 inch diameter were molded. For the very low velocity measurements, the spheres were allowed to free fall through a known distance (1 ft, 2 ft, 4 ft), striking a smooth steel plate and allowed to rebound. By equating the kinetic and potential energies before impact, the impact velocity could be determined from

$$v = \sqrt{2gH} \tag{44}$$

Similarly after impact:

$$v' = \sqrt{2gH'} \tag{45}$$

By assuming a rigid target the coefficient of restitution is

$$e = \frac{v'}{v} = \sqrt{\frac{H'}{H}} \tag{46}$$

The results of these measurements are shown as the lowest velocity circled data points in Figure 25. Targets of B/Al (0.058 in), Gr/Ep (0.040 in), and B_4C (0.25 in) were bonded to a 5/8-inch thick steel plate

and were impacted by the RTV-11 dropped from the one foot position with the results shown in Figure 26. The data for these four materials are identical within the limits of experimental error.

A 0.50-inch smooth bore gun was used to launch these spheres normal to the surface of each of these rigidly fixed targets. A 20,000 frames/sec framing camera recorded the impact and rebound velocities. The targets underwent considerable compression at impact and rebounded with an oscillating expansion and contraction about the sphere center of mass as shown in Figure 26. The framing sequence starts at the upper left corner and proceeds down the first column. The sphere is seen entering the field from the left, impacting the plate which is clamped in a small bench vise, and then rebounding to the left. The motion of the assumed center of mass was analyzed to determine the rebound velocity.

By assuming a rigid target, which exhibited no motion, Equation 46 yielded the coefficient of restitution. The results of these experiments, with data taken in the velocity range of 78 to 500 ft/sec are also shown in Figure 25. The RTV exhibits increased inelastic behavior with velocity. The measurement of e appears to be nearly independent of target material.

Auxiliary measurements of interest from these experiments are the determination of the degree of compression of the RTV against the target and the impactor/target contact time. These quantitites were determined from the high speed photographic records as seen in Figures 26 and 27. The compression was severe, reaching as much as 80% at the highest velocities, but the projectile is recovered intact after the experiment with no visible damage. At impact velocities greater than 500 feet/sec the projectile began to shatter. As seen in Figure 26 after release from the target face, the projectile has expanded to roughly twice its original length.

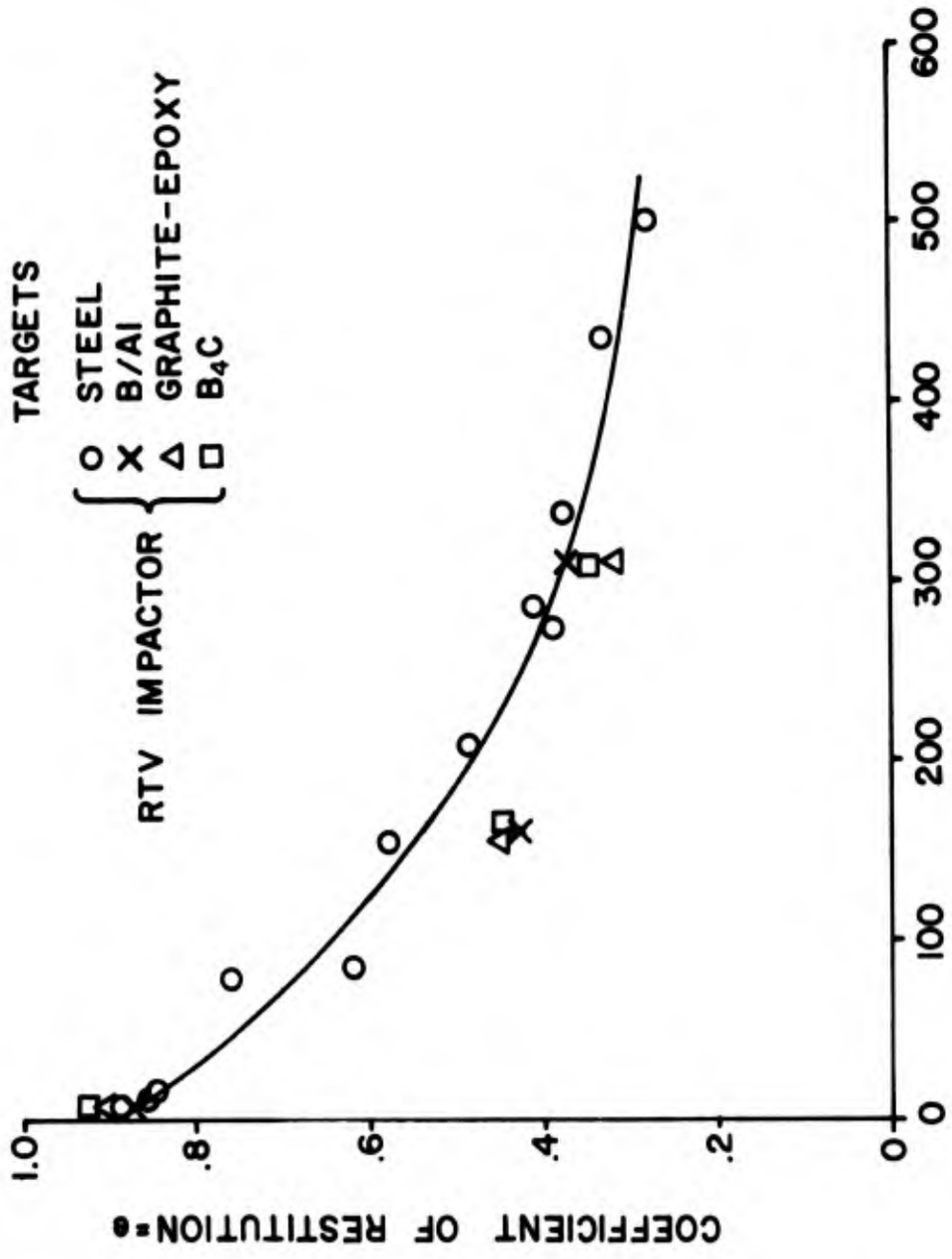

Figure 25. Measured Coefficient of Restitution

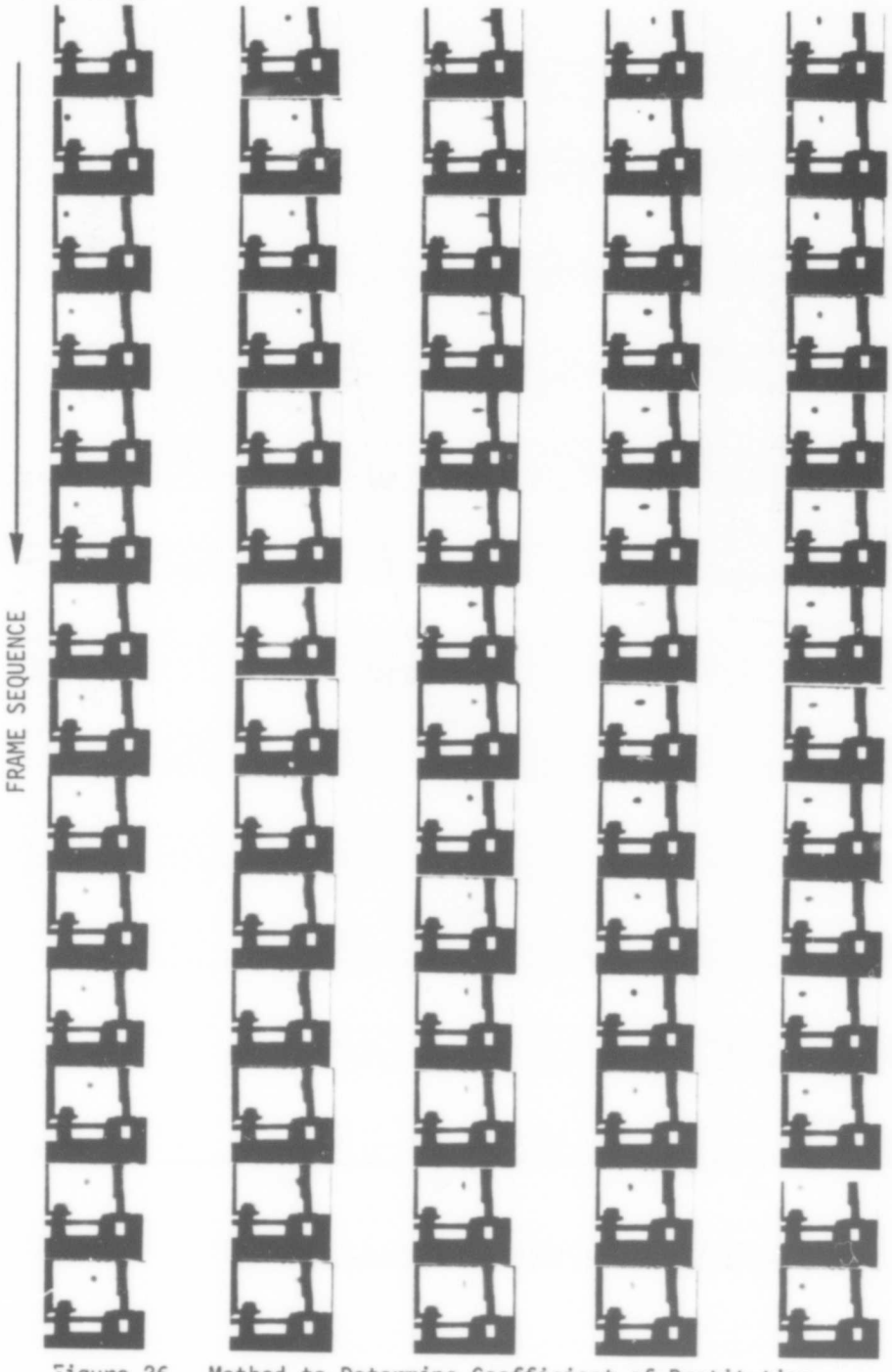

Figure 26. Method to Determine Coefficient of Restitution

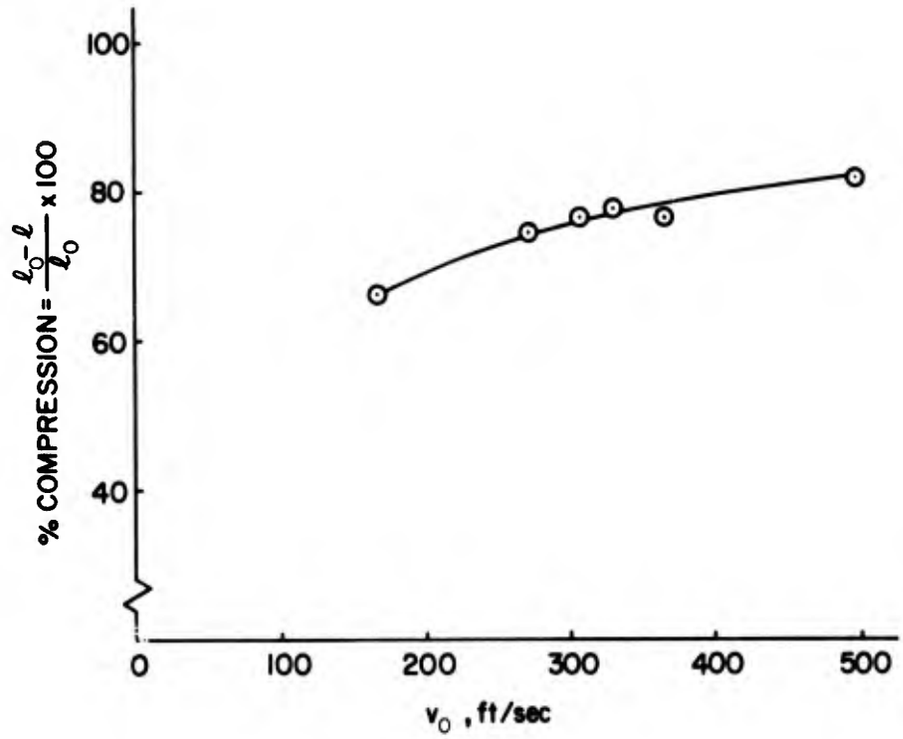

Figure 27. Compression of Projectile versus Impact Velocity

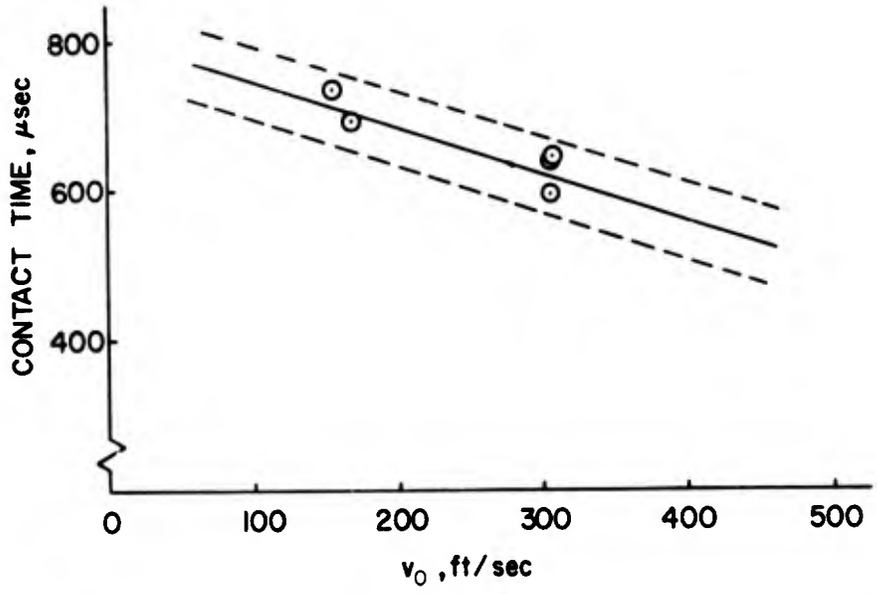

Figure 28. Contact Time versus Impact Velocity

The duration of contact between the projectile and target was determined by the framing records as in Figure 26. The results are shown in Figure 28 where the error band signifies the uncertainty in actual value arising from the long interframe time - the times of contact and departure may occur anytime within the interframe period of ~50 μ sec.

APPENDIX II

TORSIONAL VIBRATION

1. EQUIVALENT TORSIONAL STIFFNESS K

Similarly to the effective flexural stiffness k, which is defined in Equation 4, the effective torsional stiffness k_T is given by

$$k_T = \left[\frac{T}{\Phi}\right]_{X = x} \tag{47}$$

where T is the applied torque and Φ is the angle of rotation. For beams with nonuniform cross section, it is very difficult to express Φ as a function of X analytically. In this report only the case of uniform beams with narrow rectangular cross-section will be discussed. As a first approximation Φ is known to be given by the following formula

$$\Phi = \frac{TX}{I_T G} \qquad 0 \leq X \leq x \tag{48}$$

$$\Phi = \phi = \frac{Tx}{I_T G} \qquad x \leq X \leq L$$

where b is the width of the beam cross section, and

$$I_T = \frac{bh^3}{3}$$

From Equations 47 and 48 we obtain

$$k_T = \frac{GI_T}{x} = \frac{GI_T}{L}\,\frac{L}{x} \tag{49}$$

2. EFFECTIVE TORSIONAL MASS M_T

To determine the effective torsional mass M_T as a function of x, we use a similar assumption as previous employed, i.e., the maximum kinetic

energy of the beam due to torsion is equal to the maximum kinetic energy of the torsional mass-spring system. We have

$$\frac{1}{2}\int_0^L \dot{\phi}(X)^2 \, J_X \, dX = \frac{1}{2} M_T R^2 \dot{\Phi}^2 \tag{50}$$

where J_X represents the polar mass moment of inertia at X, R the radius of gyration and $\dot{\phi}$ the rate of angular rotation at X = x. Substituting $\dot{\phi}(X) = \omega_T \Phi(X)$, and $\dot{\phi} = \omega_T \phi$ into Equation 50 and making use of Equation 48, we obtain

$$M_T R^2 = \int_0^x \left(\frac{X}{x}\right)^2 J_X dX + \int_x^L J_X dx \tag{51}$$

For a uniform beam the following relations exist

$$J_X = R^2 dm = R^2 \rho \, dX \tag{52}$$

Substituting Equation 52 into Equation 51 and carrying out the integration with respect to X we obtain

$$M_T = \left(1 - \frac{2}{3}\frac{x}{L}\right) \rho L = \left(1 - \frac{2}{3}\frac{x}{L}\right) M_b \tag{53}$$

where M_b represents total mass of the beam.

3. UNCOUPLED FLEXURAL-TORSIONAL VIBRATIONS

For this case, the flexural and torsional natural frequencies are given by

$$\omega = \sqrt{\frac{k}{M}} \tag{54}$$

and

$$\omega_T = \sqrt{\frac{k_T}{J}}$$

respectively. The variation of ω_T with the point of impact is shown in Figure 29.

The initial conditions for the ensuing vibration can be derived from the theorem of conservation of linear and angular momenta and the definition of the coefficient of restitution between a particle and a rigid body. The theorem of conservation of angular momentum states that when the sum of moments of the external forces about the mass center of a rigid body is zero, the angular momentum about the mass center is conserved. Referring to Figure 3 we have

$$mzv_n = J\dot{\phi} + mzv_n' \tag{55}$$

where m v z represents the angular momentum before impact and v_n' the velocity of m after impact. Based upon the definition of the coefficient of restitution between a particle and a rigid body we have

$$V_A - v_n' = ev_n \tag{56}$$

where V_A represents the velocity of the lumped mass at the point of contact after impact. From rigid body kinematics, V_A, V and Ω are connected by the following relation

$$V_A = V + z\Omega \tag{57}$$

where Ω is the initial angular velocity. From Equations 29, 55, 56, and (57) we can express V and Ω in terms of v_n after the elimination of V_A and v_n', as

$$V = \frac{M(1+e)}{M+m(1+Mz^2/J)} v_n$$
$$\Omega = \frac{Mz}{J} V \tag{58}$$

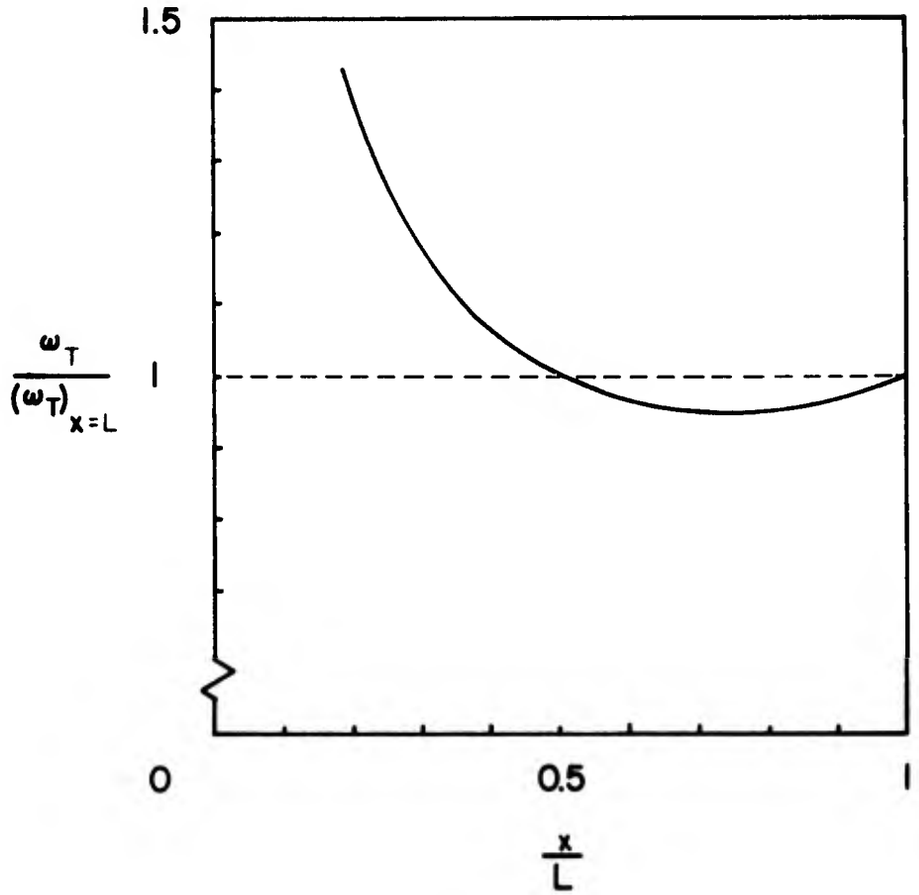

Figure 29. Natural Frequency (Torsional) versus Location of Impact

Similarly to the case of bending, the maximum angle B of the twist is given by the formula

$$B = \frac{\Omega}{\omega_T} \tag{59}$$

and the maximum shear stress for a narrow rectangular cross section under torsion is given by

$$\tau_{max} = \frac{k_T B h}{I_T} \tag{60}$$

Numerical results of ω_T from different blades are compared with experimental data in Table 4.

TABLE 4

TORSIONAL NATURAL FREQUENCIES

Matl	Dimension, in			ρ_o lb/in	x/L	ω_T, Hz	
	L	b	h			Theo	Exp
Al	3.0	1	.064	$6.374X10^{-3}$	.8	1370	1330
Ti	3.0	1	.064	$10.458X10^{-3}$	.8	835	850
B/AL	3.0	1	.064	$6.016X10^{-3}$	.8	1660	1533
Gr/Ep	3.0	1	.064	$3.936X10^{-3}$	.8	765	1133

APPENDIX III

SAMPLE CALCULATIONS

1. The velocity of the foreign object is 800 fps with an incident angle of ten degrees. The point of impact is at 0.65 L measured from the root of the blade, i.e., x = 0.65 x 9.2 = 5.98 in. The weight of the foreign object is about 3.5 oz or .22 lb and the bite of the foreign object is about 57.6%. This implies that the weight of the foreign object used to calculate the initial velocity of the blade is about .22 x .576 = 0.127 lb. The weight of the stainless steel blade is .55 lb and the effective mass M which corresponds to x/L = .65 is obtained from Equation 24 or Figure 6. The value for this case is about 0.49 x .55 = .270 lb. We now substitute m =.127, M = .270, v = 9600 in/sec, e = .3, and θ = 10° into Equation 31 and calculate the initial velocity of the blade V which is equal to 694 in/sec.

To calculate the bending natural frequency ω we use Equation 28. The stiffness k can be determined either from Equation 13 or Figure 5. Using x/L = .65 we obtain $k = 7\ EI_o/L^3$. Substituting $E = 26.8 \times 10^6$ psi, $I_o = 12 \times 10^{-4}$ in^4, L, 9.2 in, we have k = 288 lb/in. The natural frequency $\omega = \sqrt{k/M}$ = 642 rad/sec = 102 Hz is thus obtained. The maximum deflection of the blade at the point of impact can be evaluated from the formula A = V/ω = 694/642 = 1.08 in. The maximum deflection of the blade at the tip is calculated by substituting x/L = .65 and A = 1.08 in. into Equation 14. We have δ = 2.14 in. The maximum bending stress at the root can be evaluated from Equation 33:

$$\sigma_{max} = \frac{288 \times 1.08 \times 5.98 \times .125}{12 \times 10^{-4}} = 194{,}000 \text{ psi}$$

2. The initial velocity of the beam after impact, the bending natural frequency ω, and the maximum deflection of the beam can be calculated in a similar manner. The data of the foreign object and the boron aluminum beam are listed below.

Foreign Object:

$m = .35$ gram $= 7.71 \times 10^{-4}$ lb

$v = 262$ ft/sec

$\theta = 90°$

$e = 0.41$

$\frac{x}{L} = .80$

B/Al Beam:

Thickness = .057 in.

Width = .4 in.

Length = 3.8 in.

Density = 2.6 gram/cm^3

Weight = 3.69 gram $= 8.14 \times 10^{-3}$ lb

From Equation 21 or Figure 6 the effective mass M for x/L = 0.8 is

$$M = 0.474 \times 8.14 \times 10^{-3} = 3.86 \times 10^{-3} \text{ lb/g},$$

and k for x/L = 0.8 follows from Equation 9 or Figure 5,

$$k = \frac{5.85\ EI}{L^3} = \frac{5.85 \times 26.8 \times 10^6 \times 6.173 \times 10^{-6}}{(3.8)^3} = 23.70 \text{ lb/in.}$$

The area moment of inertia I_o is calculated from the given geometry as follows:

$$I_o = \frac{1}{12} (0.4)\ (0.057)^3 = 6.173 \times 10^{-6} \text{ in}^4.$$

The bending natural frequency is then obtained as

$$\omega = \sqrt{\frac{k}{M}} = \sqrt{\frac{23.70 \times 386}{3.86 \times 10^{-3}}} = 1540 \text{ rad/sec} = 244 \text{ Hz}.$$

The initial velocity V can be calculated from the formula

$$V = \frac{m\,(1 + e)}{M + m}\, v \sin\theta = 63.5 \text{ ft/sec}$$

The maximum deflection at the point of impact is given by

$$A = \frac{V}{\omega} = \frac{63.5 \times 12}{1540} = 0.488 \text{ in.}$$

and the maximum deflection at tip is obtained from Equation 7

$$\delta = 0.67$$

The maximum bending stress at the root of the blade is found to be

$$\sigma_{max} = \frac{12.15 \times .4527 \times 3.04 \times 2.85 \times 10^{-2}}{6.173 \times 10^{-6}} = 77{,}000 \text{ psi}$$

3. The natural frequency ω and the initial velocity V are obtained by similar approaches as in the preceding paragraphs 1 and 2. In our particular case

$$V = 900 \text{ in/sec}$$

$$\omega = 950 \text{ rad/sec}$$

Substituting the above data into the equation

$$\frac{V}{\omega} = A \cos \sin^{-1} \frac{A_i}{A}$$

and using $A_i = .40$ in., we obtain

$$0.95 = A \cos \sin^{-1} \frac{.40}{A}$$

By using a trial and error technique we find

$$A = 1.03 \text{ in.}$$

Substituting A = 1.03 in. into Equation 7, we obtain

$$\delta_{max} = 1.42 \text{ in.}$$

4. The torsional natural frequency can be determined from the formula

$$\omega_T = \sqrt{\frac{k_T}{J}}$$

where k_T is the torsional stiffness and J is the effective polar moment of inertia of mass. The impact data for the aluminum beam is as follows:

Density = .0976 lb/in.^{3}

Length = 3.0 in.

Width = 1 in.

Thickness = .064 in.

G = 3.864×10^6 psi

x = 0.8 length = 3.0 in.

Based upon the previous analysis we have

$$k_T = \frac{GI_T}{x}$$

where $I_T = 1/3\ bh^3$ for narrow rectangular cross-section. Using the given data we have

$$I_T = 8.74 \times 10^{-5} \text{ in.}^4$$

and

$$k_T = 1.407 \times 10^2 \text{ lb-in/radian}$$

The effective polar moment of inertia for a narrow rectangular cross section is given by

$$J = \frac{1}{12} M_T b^2$$

where M_T = torsional effective mass. From Equation 53 we have

$$M_T = \left(1 - \frac{2}{3} \frac{x}{L}\right) M_b$$

The total mass of the beam M_b is obtained by the formula

$$M_b = .0976 \times 1 \times 3 \times .064 = .0187 \text{ lb/g}$$

The torsional effective mass is then given by (for x/L = .8)

$$M_T = .467 \times .0187 = 8.73 \times 10^{-3} \text{ lb/g.}$$

The torsional frequency is then calculated as

$$\omega_T = \sqrt{\frac{1.470 \times 10^2 \times 386}{\frac{1}{12} (1)^2 \, 8.73 \times 10^{-3}}} = 8600 \text{ rad/sec} = 1370 \text{ Hz.}$$

☆U.S.Government Printing Office: 1975 — 657-020/522